

Observations of field aligned currents in the plasma sheet

Two kinds of field aligned currents generated during magnetotail convection

Kristian Snekvik



Thesis for the degree of Philosophiae Doctor (PhD)
at the University of Bergen

February, 2009

ISBN 978-82-308-0786-6978-82-308-0786-6

Bergen, Norway 2009

Preface

This synthesis and a collection of papers are submitted for the degree of philosophiae doctor (PhD) in physics at the Department of Physics and Technology, University of Bergen.

The thesis is divided into an introductory part and a part consisting of four papers submitted to international papers.

Paper I K. Snekvik, S. Haaland, N. Østgaard, H. Hasegawa, R. Nakamura, T. Takada, L. Juusola, O. Amm, F. Pitout, B. Klecker and E. A. Lucek (2007). Cluster observations of a field aligned current at the dawn flank of a bursty bulk flow. In *Annales Geophysicae*, Vol. 25, 1405-1415, url: <http://www.ann-geophys.net/25/1405/2007/angeo-25-1405-2007.pdf>

Paper II K. Snekvik, R. Nakamura, N. Østgaard, S. Haaland and A. Retinò (2008). The Hall current system revealed as a statistical significant pattern during fast flows. In *Annales Geophysicae*, Vol. 26, 3429-3437, url: <http://www.ann-geophys.net/26/3429/2008/angeo-26-3429-2008.pdf>

Paper III N. Østgaard, K. Snekvik, A. L. Borg, A. Åsnes, A. Pedersen, M. Øieroset and T. Phan (2008). Can magnetotail reconnection produce the observed ionospheric observations? Submitted to *Journal of Geophysical Research*

Paper IV K. Snekvik, L. Juusola, N. Østgaard and O. Amm (2009). Reconnection Hall current system observed in the magnetotail and in the ionosphere Submitted to *Geophysical Research Letters*

I have also contributed to the following papers. They are not part of the thesis.

Paper A A. S. Sharma, R. Nakamura, A. Runov, E. E. Grigorenko, H. Hasegawa, M. Hoshino, P. Louarn, C. J. Owen, A. Petrukovich, J.-A. Sauvaud, V. S. Semenov, V. A. Sergeev, B. U. Ö. Sonnerup, L. M. Zelenyi, G. Fruit, S. Haaland, H. Malova, and K. Snekvik. (2008). Transient and localized processes in the magnetotail: a review. In *Annales Geophysicae*, Vol. 26, 955-1006, url: <http://www.ann-geophys.net/26/955/2008/angeo-26-955-2008.pdf>

Paper B T. Takada, R. Nakamura, L. Juusola, O. Amm, W. Baumjohann, M. Volwerk, A. Matsuoka, B. Klecker, K. Snekvik, C. J. Owen, A. N. Fazakerley, H. U. Frey, H. Rème, E. A. Lucek and C. Carr. (2008). Local field-aligned currents in the magnetotail and ionosphere as observed by a Cluster, Double Star and MIRACLE conjunction. In *Journal of Geophysical Research*, Vol. 113, A07S20, doi: 10.1029/1007JA012759

This work is funded by the Norwegian Research Council project *Investigation of Magnetosphere-Ionosphere Coupling using Cluster Data* with project number 170844.

Contents

Acknowledgements	vii
1 Introduction	1
1.1 Historical development of our understanding of field aligned currents .	2
2 Theory for magnetospheric convection	7
2.1 Basic theory	7
2.2 The Dungey cycle	9
2.3 The magnetotail	11
2.4 The pressure crisis	12
2.4.1 Depleted flux tubes	13
2.4.2 Near-Earth reconnection	14
3 Generation of field aligned currents	17
3.1 Fast flows and FACs	17
3.2 Reconnection and Hall currents	19
4 Observations	23
4.1 Fast flows	23
4.1.1 Transport of plasma and magnetic flux in the near-Earth plasma sheet	23
4.1.2 Earthward boundary of fast flows	26
4.1.3 Structure of fast flows	27
4.2 Near-Earth reconnection	31
4.3 Field aligned currents in the ionosphere and the magnetotail compared	35
5 Cluster	39
5.1 Data products	41
6 Single and multi spacecraft analysis methods	43
6.1 Plasma β	44
6.2 Harris current sheet	45
6.3 Reconstruction of the current sheet	46
6.4 Current sheet orientation	46

6.5	Boundary normal	47
6.6	deHoffmann-Teller analysis	47
6.7	Curved boundaries	47
7	Summary of papers	49
7.1	Paper I: Cluster observations of a field aligned current at the dawn flank of a bursty bulk flow	49
7.2	Paper II: The Hall current system revealed as a statistical significant pattern during fast flows	50
7.3	Paper III: Can magnetotail reconnection produce the observed ionospheric observations?	51
7.4	Paper IV: Reconnection Hall current system observed in the magnetotail and in the ionosphere	52
	Bibliography	55
	A Abbreviations and Acronyms	61
	Index	62
	Paper I Cluster observations of a field aligned current at the dawn flank of a bursty bulk flow	67
	Paper II The Hall current system revealed as a statistical significant pattern during fast flows	81
	Paper III Can magnetotail reconnection produce the observed ionospheric observations?	93
	Paper IV Reconnection Hall current system observed in the magnetotail and in the ionosphere	113

Acknowledgements

I have been privileged to work with a number of very skilled people during the past three years as a PhD student. First of all I would like to express gratitude to my supervisor Nikolai Østgaard. Without his reminders of keeping the PhD schedule, I would not been able to finish in time. In the last year we have also worked closely together, which I have greatly appreciated.

Stein Haaland is my co-supervisor and is an expert on Cluster analysis methods. He has taught me a number of techniques, which have been essential for my research. For that, and everything else he has done for me, I am sincerely grateful.

In 2006 and 2007 I spent the autumn at the Space Research Institute in Graz in Austria. Of major importance for my work was the cooperation with Rumi Nakamura. Her interpretational skills are exceptional and were crucial for my two first articles. Other individuals I met at the Space Research Institute who deserves acknowledgements for many interesting discussions are Taku Takada, Andrei Runov, Liisa Juusola, Alessandro Retinò and Sergey Apatenkov. I would also like to thank Bruno Besser, Zoltàn Vörös and Magda Delva for making sure that I had some social life apart from science.

I thank all the staff and students in the Space Physics Group in Bergen for an excellent social environment. I am particularly thankful to Karl Magnus Laundal and Marianne Daae. Their enthusiasm and interest for my work has been a great encouragement.

At last I would like to thank Marita Sørbø, Karl Magnus Laundal, Sigurd Henrik Teigen and Bjørg Snekvik for proof reading of this document.

Bergen, February 2009

Kristian Snekvik

Chapter 1

Introduction

The motivation for this thesis is to increase our understanding of the generation mechanisms for field aligned currents (FACs) in the magnetosphere. We have focused on two generation mechanisms in the magnetotail, these are reconnection and fast flows. Both mechanisms are related to magnetospheric convection. The study is based on measurements by the four Cluster satellites. They have a polar orbit with perigee at $4 R_E$ and apogee at $19.6 R_E$, as illustrated in Fig. 1.1.

Paper I presents an event study of a fast earthward flow known as a bursty bulk flow. Detailed observations that show how a FAC is generated by the flow are presented. It is shown that the observations agree with a theoretical model which predicts that plasma can be transported earthward in the form of depleted flux tubes. Paper II is a statistical paper where another kind of FAC is observed. This FAC can best be understood in terms of the Hall current system which is produced in the reconnection region. Particle measurements during reconnection are studied in Paper III. It is shown that particle acceleration in the reconnection region alone, would give little or no aurora in the ionosphere, despite the FACs produced there. In Paper IV magnetospheric observations of the Hall current system are compared with measurements from ground magnetometers. The results indicate that the Hall current system closed through the ionosphere.

Convection in the magnetosphere in general and in the magnetotail in particular, is introduced in Chapter 2. A general description of reconnection and depleted flux tubes is also given there. Chapter 3 focuses on the generation mechanisms for FACs related to reconnection and fast flows. Observations of fast flows, near-Earth reconnection and FACs are described in Chapter 4. Next, a brief description of the Cluster satellites is given in Chapter 5, followed by an account of the methods we have used in our data analysis in Chapter 6. A list of abbreviations and an index are included at the end. We begin with a historical outline of the development of our understanding of FACs from the late nineteenth century until the satellite era. The first part is about Kristian Birkeland and is mainly built on *Egeland* (1984), while the second part is based on *Dessler* (1984).

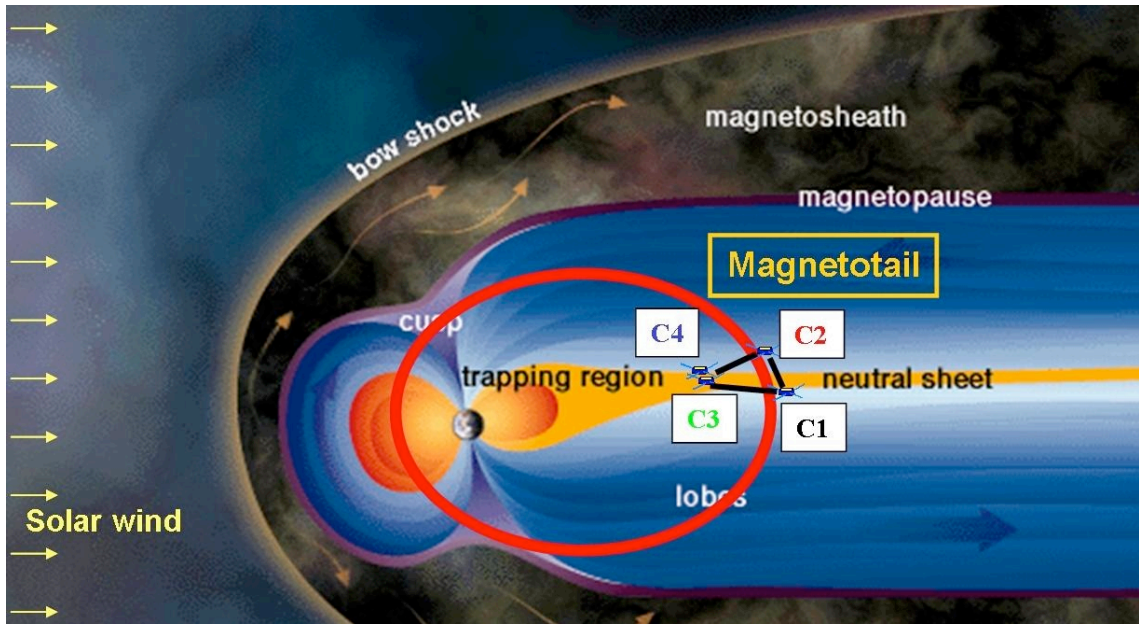


Fig. 1.1. Illustration of the Cluster orbit when the apogee of their orbit is in the plasma sheet on the nightside of the Earth. [© European Space Agency]

1.1 Historical development of our understanding of field aligned currents

The early measurements of geomagnetic activity were limited to what could be inferred from the ground. This included measurements of the ground magnetic field and observations of northern lights. The scientific understanding of these phenomena was poor until the beginning of the twentieth century, when Kristian Birkeland's (1867-1917) experiments contributed to great progress in auroral science. Earlier, in 1741, Hiorter and Celsius discovered that auroral activity and geomagnetic disturbances were closely related. In 1881 Fritz found that the northern light has maximum intensity close to 23° co-latitude from the magnetic poles.

Birkeland (1908, 1913) studied magnetic disturbances in ground magnetometers, and argued that they could be caused by “equivalent” electric currents in the atmosphere. (The ionosphere was not discovered at that time.) He found that the geomagnetic disturbances in the auroral zone were very different from the disturbances near the equator and called them polar elementary storms, in contrast to the equatorial perturbations. Today, polar elementary storms are better known as substorms. The “equivalent” currents formed patterns which were similar during all substorms. These substorm currents were estimated to be of the order of 1 MA; which is a reference value used even today. Birkeland proposed a model where electrons originating from the Sun, spiralled up and down the magnetic field lines in the

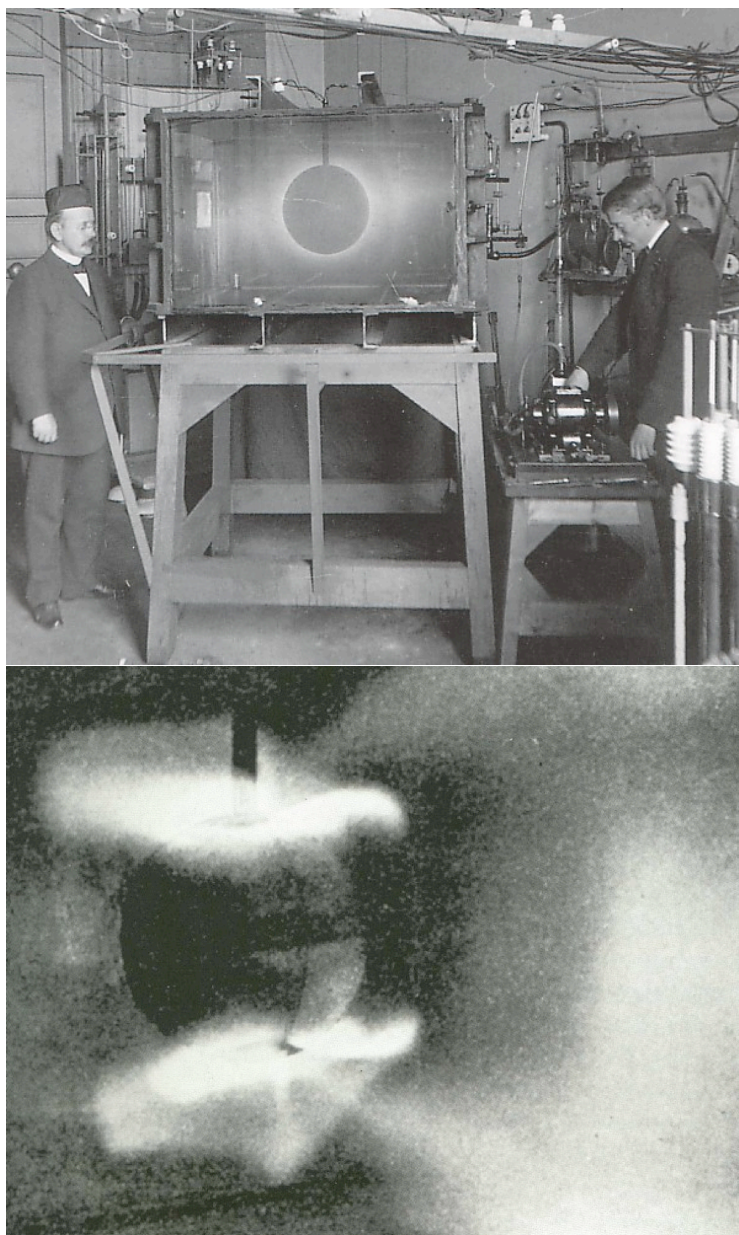


Fig. 1.2. Top: Kristian Birkeland (left) with the terrella experiment. Bottom: Artificial aurora made in the terrella experiment. [*The Norwegian Museum of Science and Technology*]

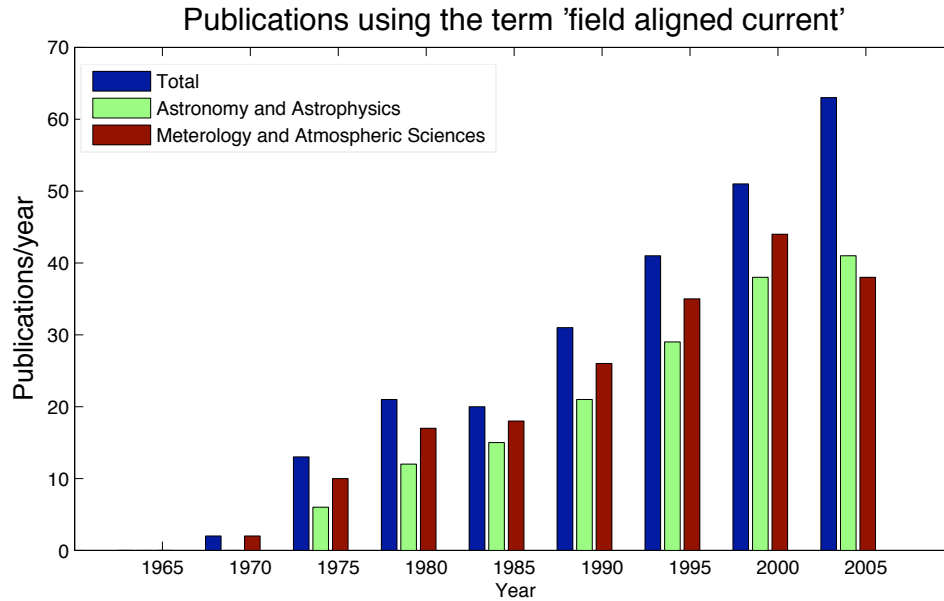


Fig. 1.3. Number of publications using the term “field aligned current” in total (blue), in Astronomy and Astrophysics (green), and in Meteorology and Atmospheric Sciences (brown). Note that the same article could be counted in more than one category. The values are averages over intervals of five years [ISI Web of Knowledge]

form of field aligned currents, to feed the horizontal currents and cause the polar aurora. Originally, he got this idea by directing beams of electrons inside a vacuum chamber towards a sphere with a dipole field. By coating the globe with fluorescent painting, he was able to see where the electrons impinged on it. The electrons hit the surface of the sphere to create two rings of artificial aurora around the poles. This was called the terrella experiment and is illustrated in Fig. 1.2.

The theories of Birkeland were neglected for many years. Partly because one of the leading scientists at that time, Lord Kelvin (1824-1907), rejected his theories and wrote: “The supposed connection between geomagnetic storms and sunspots is unreal.” Another scientist, Sydney Chapman (1888-1970), derived an alternative theory where the magnetic disturbances at the ground could be explained by horizontal currents in the ionosphere alone. This theory was very attractive for many scientists because it was mathematically exact. After 1939 a younger scientist, Hannes Olof Gösta Alfvén(1908-1995), attempted to revive Birkeland theories (*Dessler and Wilcox, 1970*). However, his ideas were not accepted before the start of the satellite era.

When measurements from satellites became available, transverse magnetic field disturbances in the auroral zone were reported (*Cummings and Dessler, 1967*, and references therein). The common explanation was that they were due to hydro-magnetic waves. However, *Cummings and Dessler (1967)* pointed out that many

observations could not be explained by hydromagnetic waves. As an alternative they proposed that the field aligned currents of Birkeland were the cause of the magnetic disturbances. This seems to be the breakthrough for the theory of field aligned currents or Birkeland currents. After 1967 the number of publications on the subject have increased every year, as shown in Fig. 1.3.

It is amazing that Birkeland got so many aspects of his auroral theories correct. Especially when we consider that he did not know about the solar wind, the magnetosphere or the solar wind. Today, it is known that field aligned currents encircle the auroral oval as a more or less permanent phenomenon. The FACs do not only consist of electrons from the Sun, but also electrons from the ionosphere. However, the energy that drives the FACs, ultimately comes from the Sun. This drives a global convection of plasma in the magnetosphere. It is just a small part of this convection and the FACs associated with it, that will be studied here. The next chapter gives an overview of this convection.

Chapter 2

Theory for magnetospheric convection

Some basic theory related to convection will be presented in the first section. Two concepts which many of our interpretations are built on, are explained, namely the frozen-in approximation and magnetic reconnection. Sect. 2.2 is about the transport of plasma and magnetic field in the magnetosphere known as the Dungey cycle. An overview of the magnetotail is given in Sect. 2.3. A major problem with the convection in the magnetotail is the pressure crisis. This is explained in the Sect. 2.4, and two possible solutions for the problem are presented.

2.1 Basic theory

The magnetosphere as well as the interplanetary space is filled with very hot particles with temperatures ranging from hundreds of thousands to tens of millions Kelvin. Since space plasmas are collision-less, the important force on the particles is the Lorentz force - the combined force from the electric and magnetic fields. But every moving particle is also in itself a source of such fields. This makes it hard to evaluate how the plasma will develop over time. Instead of considering every single particle, one can study the distribution of the particles. This is given by the phase space density:

$$f_p(\mathbf{r}, \mathbf{v}) = \frac{dN}{d\mathbf{r}d\mathbf{v}}, \quad (2.1)$$

where dN is the number of particles with positions between \mathbf{r} and $\mathbf{r}+d\mathbf{r}$ and velocities between \mathbf{v} and $\mathbf{v} + d\mathbf{v}$. An equation for how the phase space density develops with time is given by the Vlasov equation (*Baumjohann and Treumann, 1997*):

$$\frac{\partial}{\partial t} f + \mathbf{v} \cdot \nabla f + \frac{q}{m} (\mathbf{E} + \mathbf{v} \times \mathbf{B}) \cdot \nabla_{\mathbf{v}} f = 0, \quad (2.2)$$

where \mathbf{E} is the electric field, \mathbf{B} is the magnetic field and q and m are the charge and mass of the particles, respectively. This equation expresses that f is constant when

we follow the plasma in phase space. Without going too much into details one can show that Vlasov equation can be reduced to

$$(\mathbf{E} + \mathbf{v} \times \mathbf{B}) \cdot \nabla_{\mathbf{v}} f \approx 0. \quad (2.3)$$

This approximation holds reasonably well when the gyro radius and the gyro period of the particles are much smaller than typical lengths and times which give large changes in the distribution function. In addition, the electric field parallel with the magnetic field must be assumed to be small.

Equation 2.3 implies that the electric field vanish in a reference frame moving with $\mathbf{u}_{\perp} = \mathbf{E} \times \mathbf{B} / (B^2)$. Another consequence is that the distribution function will be gyrotropic in this reference frame (*Clemmow and Dougherty, 1969*), i.e. symmetric around the field lines. Since the gyro radius is dependent on the energy of the particles, the approximation holds better for cold than hot particles. When this relation holds for the major part of the particle population, it is called the frozen-in approximation. In that case \mathbf{u}_{\perp} is the average velocity of the particles perpendicular to the magnetic field. \mathbf{u}_{\perp} is often called the convection velocity or the $\mathbf{E} \times \mathbf{B}$ drift. The frozen-in approximation allows a magnetic field line to be imagined as a rope which is glued to the plasma. The plasma is free to move parallel with the rope, but is restricted to follow the rope in the perpendicular directions. Another consequence of the frozen-in approximation is that two different volumes of plasma cannot mix. This is important when convection in the magnetotail will be discussed later in this chapter.

When the frozen-in approximation holds for both ions and electrons, the one-fluid momentum equation can be written as (*Parks, 2004*):

$$\rho_m \frac{d}{dt} \mathbf{u}_{\perp} = -\nabla_{\perp} p_{\perp} - (p_{\parallel} - p_{\perp})(\mathbf{b} \cdot \nabla) \mathbf{b} + \mathbf{j} \times \mathbf{B} \quad (2.4)$$

$$\rho_m \frac{d}{dt} \mathbf{u}_{\parallel} = -\nabla_{\parallel} p_{\parallel} + (p_{\parallel} - p_{\perp}) \frac{\nabla_{\parallel} B}{B}, \quad (2.5)$$

where ρ_m is the mass density, p is the pressure, \mathbf{b} is the magnetic field unit vector and \mathbf{j} is the current density. \perp and \parallel denote perpendicular and parallel components, respectively. Sometimes another form of the perpendicular momentum equation is more illuminating. By using Ampères law and assuming isotropic pressure, Eq. 2.4 can be written as

$$\rho_m \frac{d}{dt} \mathbf{u}_{\perp} = -\nabla_{\perp} \left(p + \frac{B^2}{2\mu_0} \right) - \frac{B^2}{\mu_0} \frac{\hat{\mathbf{n}}}{R} \quad (2.6)$$

The last term is the curvature force, where $\hat{\mathbf{n}}$ is a unit vector pointing away from the center of curvature along the curvature radius, R . This force tries to straighten the magnetic field lines.

Magnetic reconnection

As we will see below, the frozen-in approximation is very useful to understand the transport of mass and flux in the magnetosphere. Still, some of the most interesting

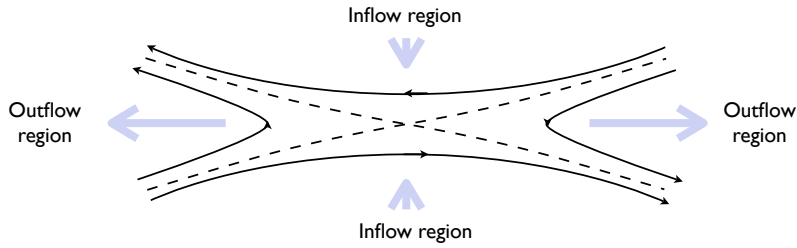


Fig. 2.1. The basic geometry of a the reconnection region.

phenomena takes place when the conditions for this approximation breaks. One of these phenomena is magnetic reconnection. Figure 2.1 shows the basic geometry of reconnection. The dashed lines are called the separatrices because they separate magnetic field lines with different topology. The center of the figure, where the dashed lines meet, is the X-line or neutral line. The upper and lower quadrants are the inflow regions where plasma and magnetic field lines flow towards the X-line. When magnetic field lines of different polarity are forced sufficiently close together, the frozen-in approximation will not be valid any more. The magnetic field lines can be “split” in two and connect to the other field line. This results in the strongly curved magnetic field lines in the left and right parts of the figure. As seen from Eq. 2.6, this implies a curvature force, which accelerates the plasma away from the X-line.

2.2 The Dungey cycle

With the concepts of frozen-in field lines and reconnection, the circulation of plasma in the magnetosphere can be explained. Figure 2.2 illustrates this. Interplanetary magnetic field (IMF) lines arrive from the left with the solar wind. When the IMF has a southward component, an oppositely directed geomagnetic field line at the front side of the magnetosphere can connect to the IMF. It will then become what is called an open field line, as opposed to closed field lines which are entirely inside the magnetosphere. Since one end of the field line is immersed in the solar wind, the field line is pulled tailward. The part of the field line above the ionosphere moves across the polar cap from the dayside to the nightside as shown in the inset in Fig. 2.2. At the nightside the open field lines are “piled up” in the magnetospheric lobes. As more flux is added, the field lines will slowly move towards the center where reconnection again takes place. To close the cycle the magnetic field lines must be transported back to the dayside inside the magnetosphere. How this transport of closed field lines takes place in the magnetotail will be one of the major topic for this thesis. This form of magnetospheric convection was first proposed by *Dungey* (1961) and is often called the Dungey cycle.

The coordinate system in the lower left corner of Fig. 2.2 will be used throughout

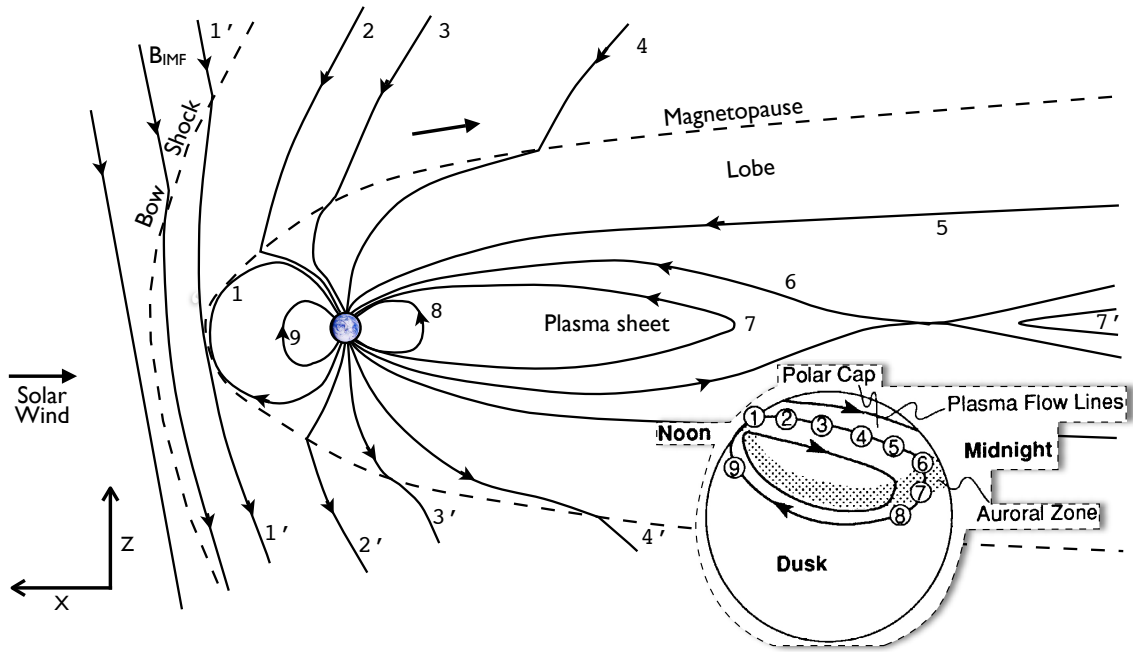


Fig. 2.2. The Dungey cycle: Flow of plasma within the magnetosphere driven by magnetic reconnection. The numbers show how a magnetic field line moves after it connects with the solar wind (1), is dragged over the polar cap to the magnetotail (2-5) where it reconnects to another geomagnetic field line (6) and then moves back to the dayside inside the magnetosphere (7-9). The inset shows the ionospheric footprints of the field lines. Adopted from *Hughes (1995)*.

the text, unless otherwise stated. The origin is in the center of the Earth, the X-axis is pointing towards the Sun and the Z-axis is pointing northward. There are some variations in how the “northward” direction is determined. In the Geocentric Solar Magnetospheric (GSM) coordinate system, the Z-axis is determined from the component of the dipole axis which is perpendicular to the Sun-Earth line. In the Geocentric Solar Ecliptic (GSE) coordinate system, the Z-axis is normal to the Earth’s orbital velocity and the Sun-Earth line. A slightly modified version of GSM will sometimes be referred to in the text. This is called aberrated GSM (AGSM) and adjusts for the orbital speed of the Earth V_E . This coordinate system is obtained by rotating GSM with an angle α clockwise around the Z-axis. $\alpha = \tan^{-1}(V_E/V_{SW})$, where V_{SW} is the solar wind speed. It is assumed that the solar wind flows radially out from the Sun.

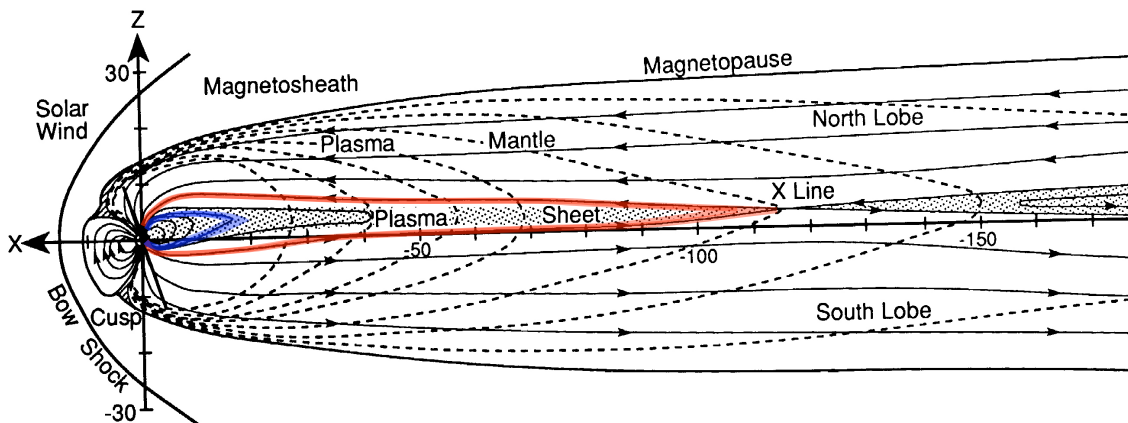


Fig. 2.3. The magnetotail. Solid lines are the magnetic field and dashed lines are trajectories of particles with different energy. The red line indicates a flux tube which has just reconnected at the X-line. The blue line is a flux tube closer to the Earth. Adapted from *Hughes* (1995)

2.3 The magnetotail

Figure 2.3 shows a more realistic model of the magnetotail. Observations indicate that the X-line is placed about $100 R_E$ from the Earth (e.g. *Slavin et al.*, 1985). This X-line is often called the distant X-line of reasons we will come back to. The closed field lines on the earthward side of the X-line and between the lobes constitute the plasma sheet. The distant X-line acts like a velocity filter (*Hughes*, 1995) as illustrated by the dashed lined in Fig. 2.3. The dashed lines illustrate the trajectories of particles which stream tailward along the lobe field lines. All the particles will have the same $\mathbf{E} \times \mathbf{B}$ drift towards the plasma sheet, but their parallel velocity will vary. The fastest particles will pass the X-line before they have reached the plasma sheet. Slower particles, which enter the plasma sheet on the earthward side of the X-line, will be captured on closed field lines.

Figure 2.4 shows an illustration of the plasma sheet. The region in the center is called the central plasma sheet (CPS). It is characterised by hot and relatively dense plasma and weak magnetic field. The part of the CPS where the magnetic field is weakest, is called the neutral sheet. Between the CPS and the lobes is the plasma sheet boundary layer (PSBL). The values of the plasma density and temperature in the PSBL lie between the corresponding CPS and lobe values. Lobe particles which enter the plasma sheet on the earthward side of the distant X-line will follow a Speiser-type orbit and be accelerated in the acceleration region (*Hughes*, 1995) (Fig. 2.4). They will then be ejected along the field lines with a large field aligned component to their velocity. When they reach the strong magnetic field near the Earth, most of them will be reflected and stream back along the field again. These earthward and tailward streaming particles are characteristic for the PSBL. If there

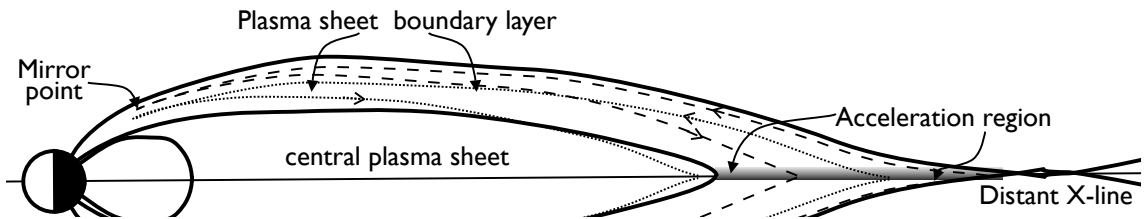


Fig. 2.4. The plasma sheet boundary layer consists of particles which have drifted in from the lobes and been accelerated in a portion of the plasma sheet earthward of the distant X-line. The dashed and the dotted line show the trajectories of two particles as they stream along the magnetic field lines and convect towards the central plasma sheet. Adapted from *Hughes* (1995).

is an electric field across the tail, the particles will also convect slowly towards the CPS. Later in this thesis we will refer to these field aligned moving particles as field aligned beams (FABs).

2.4 The pressure crisis

The red line in Fig. 2.3 shows a flux tube which has just reconnected, and the blue line is the same flux tube after it has convected towards the Earth. A flux tube is a volume where the surface is everywhere parallel with the magnetic field lines, so that every cross section of the flux tube contains the same magnetic flux. *Erickson and Wolf* (1980) have pointed out that if the flux tube convects adiabatically, the pressure in the flux tube would increase to unrealistically high values. The adiabatic relation between the volumes and the pressures of the two flux tubes is

$$\frac{p_2}{p_1} = \left(\frac{V_1}{V_2} \right)^{\frac{5}{3}}. \quad (2.7)$$

Observations showed that the pressure increases with a factor between two and four from $60 R_E$ to $10 R_E$. The corresponding decrease of the volume of the flux tube would be between a factor 1.5 and 2.3 according to the adiabatic relation. *Erickson and Wolf* (1980) argued that it is not possible to construct a magnetotail where the volumes of the fluxtubes have so little variation with the distance from the Earth. This is called the pressure crisis.

The pressure-balance inconsistency suggests that slow, steady and uniform convection in the Earth's plasma sheet occurs only rarely, if ever (*Chen and Wolf*, 1999). In the following sections we will describe two processes for avoiding the pressure crisis. The processes are

1. Depleted flux tubes. The flux tube starts out with lower pressure than the surrounding plasma and can therefore propagate further earthward before the pressure crisis occurs.

2. Near-Earth reconnection. If an X-line occurs closer to the Earth than the distant X-line, the pressure crisis is less likely to happen.

In the next chapter mechanisms for the generation of field aligned current in the magnetotail related to these processes will be presented. The depleted flux tube model is relevant for Paper I, where observations which agrees with this theory are presented.

2.4.1 Depleted flux tubes

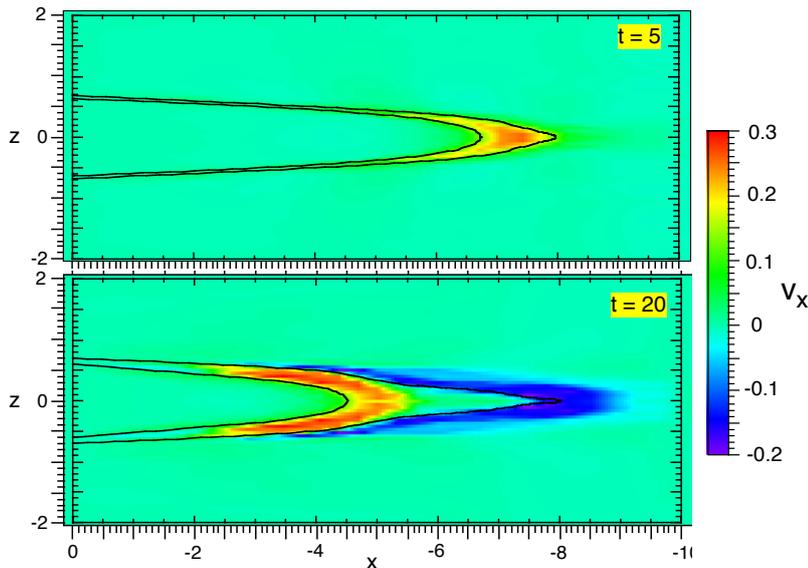


Fig. 2.5. Plasma velocities at $t=5$ (125 s) and at $t=20$ (500 s) after the depleted flux tube is formed. From *Birn et al.* (2004)

Pontius and Wolf (1990) have suggested that the convection in the magnetotail may take the form of underpopulated flux tubes, also called bubbles. Such bubbles start out with lower density and pressure than the surrounding medium. Pressure equilibrium in the plasma sheet is quickly restored by a strengthened magnetic field inside the depleted flux tubes, so that the sum of magnetic pressure and thermal pressure is the same as in the neighbouring flux tubes. The increased magnetic field inside the bubble, will increase the curvature force in Eq. 2.6. This force is usually balanced by the pressure gradients in the magnetotail, but will now accelerate the bubble earthward. In Chapter 4 observations of a type of fast flows in the plasma sheet called bursty bulk flows, will be presented. Bursty bulk flows are believed to be the major contributor to convection in the plasma sheet. *Chen and Wolf* (1993) have argued that the bursty bulk flows are bubbles in the Earth's plasma sheet.

Birn et al. (2004) performed a three dimensional MHD simulation of the propagation and dynamics of a depleted flux tube. The earthward propagation of the

bubble is shown in Fig. 2.5. After the initial density depletion, pressure equilibrium is quickly re-established. Close to the neutral sheet this is mainly caused by increased temperature and B_Z , while B_X increases mostly in the outer parts of the flux tube. Surrounding plasma will fill the volume left by the earthward moving flux tube, as seen in the bottom panel in Fig. 2.5. At the leading edge of the flow, there will be a strong dipolarization, which reduces in the tailward parts of the flux tube.

Reconnection causes low density lobe field lines to reconnect and become closed plasma sheet field lines. Reconnection is therefore a likely source of the depleted flux tubes. In their simulation *Birn et al.* (2004) showed that an earthward moving flux tube that is not depleted will quickly stop. Therefore, reconnection without depletion is not sufficient for the magnetotail convection.

2.4.2 Near-Earth reconnection

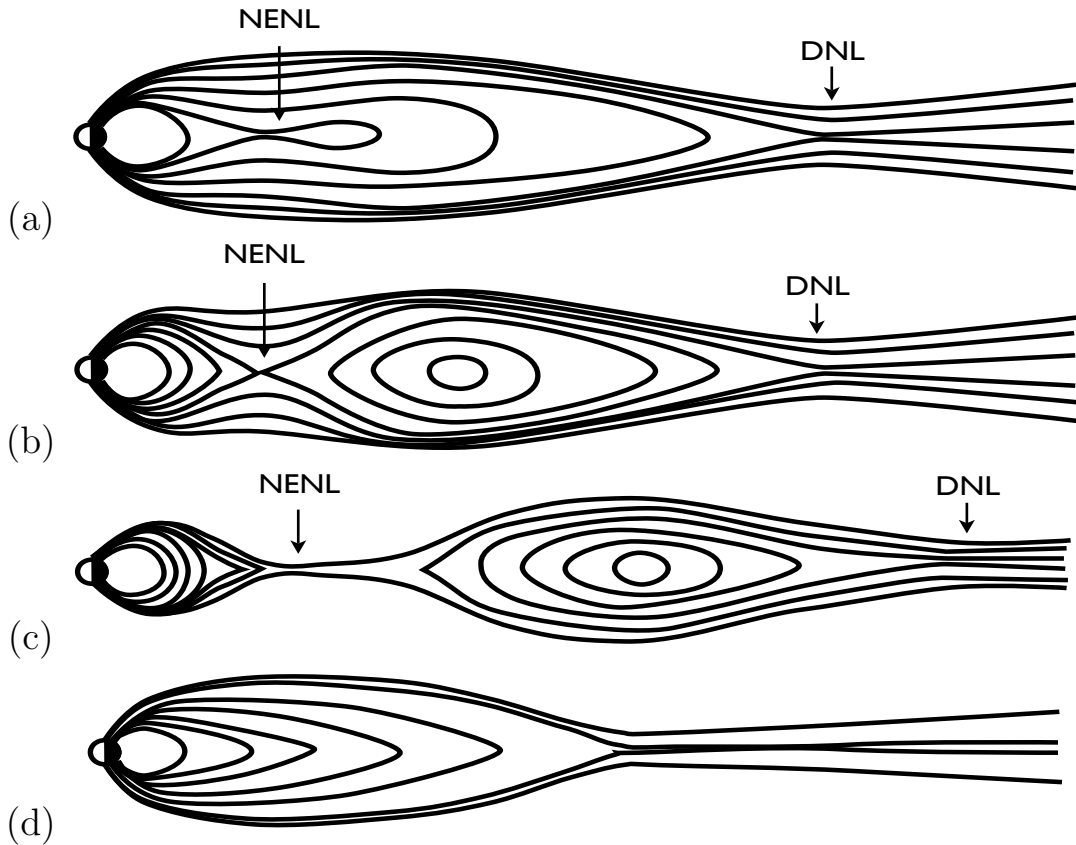


Fig. 2.6. Reconnection at the near earth neutral line (NENL) and the distant neutral line (DNL). Adapted from *Hones Jr* (1984)

Another method to avoid the pressure crisis is if reconnection takes place closer to the Earth than the distant X-line. In this section we will only present the large scale

characteristics of near-Earth reconnection. More detailed discussions of processes in and around the X-line are left to Sect. 3.2 and Sect. 4.2.

When the open magnetic field lines with labels 2-4 in Fig. 2.2 are added to the lobes, the magnetic flux in the lobes will increase. Since the open magnetic field lines are more perpendicular to the Sun-Earth line than the pre-existing field lines, the solar wind component normal to the magnetopause will increase (*Fairfield, 1985*). The lobes are pressed towards the equatorial plane resulting in current sheet thinning (*McPherron et al., 1973*). This can lead to reconnection in the near earth tail (*Baker et al., 1996*). Observations indicate that this normally takes place for $-20R_E > X_{\text{GSM}} > -30R_E$ (see Sect. 4.2).

As can be seen from Fig. 2.6, near-Earth reconnection has large consequences for the tail geometry. It starts out at closed field lines (Fig. 2.6a). This creates a magnetic structure tailward of the X-line called a plasmoid. It consists of closed loops of magnetic field lines. As reconnection continues, the plasmoid grows (Fig. 2.6b). When open field lines start to reconnect (Fig. 2.6c), the plasmoid is ejected tailward. In the end, the near-Earth neutral line retreats tailward and becomes the distant neutral line (Fig. 2.6d).

The scenario may not evolve exactly as described above. It has been argued that multiple X-lines may form at different times and at different distances from the Earth (*Slavin et al., 2003*, and references therein). In addition, if the tail magnetic field has a B_Y component, the magnetic field lines will create flux ropes instead of plasmoids. The resulting geometries can become quite complicated (*Hughes and Sibeck, 1987*). The X-line is also likely to have a finite width of $2-3 R_E$ (see Chapter 4), so that multiple X-lines may also be spread azimuthally as well as radially in the tail (*Sergeev et al., 2001*).

Chapter 3

Generation of field aligned currents

Currents in space plasmas are essentially divergence free. This allows one to construct loops where the current is constant everywhere. In areas where $\mathbf{E} \cdot \mathbf{j} < 0$ flows from the plasma to the magnetic field, and opposite when $\mathbf{E} \cdot \mathbf{j} > 0$. The integral of $\mathbf{E} \cdot \mathbf{j}$ around the closed loop, is equal to the rate of change of the magnetic flux through the loop (*Cowley, 2000*). Thus, the integral becomes zero in a steady state.

When part of the current loop pass through the ionosphere, the ionospheric Pedersen current will be a “load” where energy is transferred from the magnetic field to the plasma. This means that the magnetospheric part of the current loop must be a generator.

Both fast flows in the plasma sheet and reconnection are believed to result in field aligned currents. The theory for this FAC generation will be outlined below.

3.1 Fast flows and FACs

There are at least four different processes discussed in the literature related to the generation of field aligned currents by fast flows in the magnetotail. Common for many of these processes is that the flow channel acts like an obstacle for the cross tail current, so that it becomes diverted along the magnetic field lines. This is shown schematically in Fig. 3.1. This current system is often called a current wedge.

From Eq. 2.4 the perpendicular current is

$$\mathbf{j}_{\perp} = \rho_m \frac{\mathbf{B}}{B^2} \times \frac{d\mathbf{u}_{\perp}}{dt} + \frac{\mathbf{B}}{B^2} \times \nabla p, \quad (3.1)$$

where the thermal pressure is assumed to be isotropic. The first term is called the inertial current, and the second term is the diamagnetic current. In the plasma sheet the pressure gradient is mainly in the Z -direction, but it will also have a smaller component towards the Earth. The pressure gradient gives rise to the cross

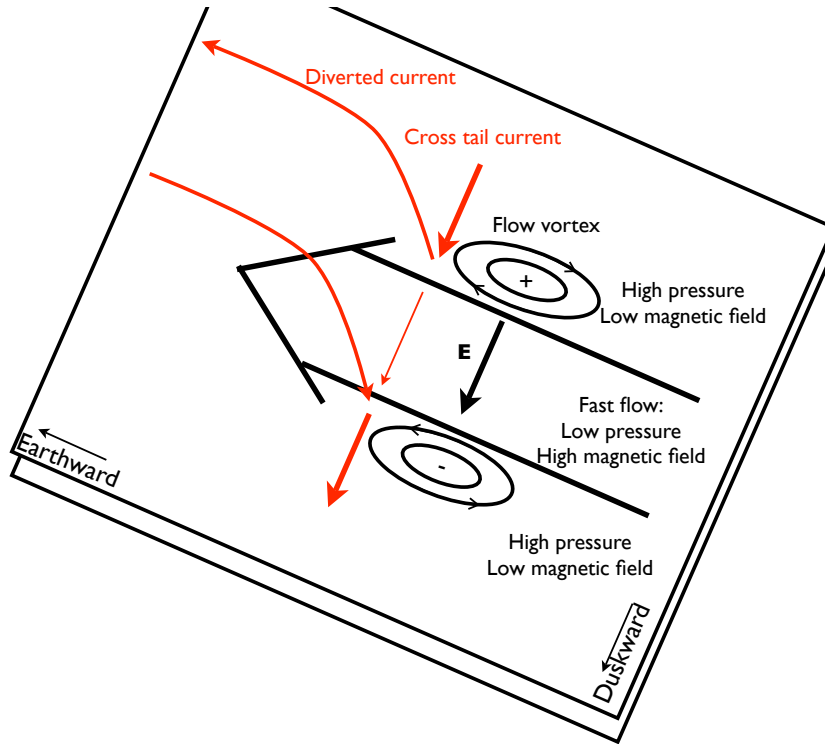


Fig. 3.1. An earthward flowchannel and its associated current wedge.

tail current. In the underpopulated flux tube discussed in Sect. 2.4.1, there is lower thermal pressure leading to a smaller pressure gradient. Together with higher magnetic field, the diamagnetic current will be smaller inside the flux tube, compared to the neighbouring flux tubes. Part of the cross tail current must therefore be diverted. When the flux tube is accelerated towards the Earth, $du/dt > 0$ results in inertial currents which partially cancel this effect (*Pontius and Wolf, 1990*).

Birn et al. (2004) reported that flow vortices were created at the flanks of the depleted flux tube in their simulation. The electric field converged and diverged at the dawn and dusk flanks, respectively, corresponding to space charges (Fig. 3.1). However, the contribution of the space charges to the FACs was negligible in their simulation, in accordance with that plasmas should be quasi-neutral. The dominant contribution to the FACs was the twisting of the magnetic field due to the flow vortices. It varied between 10^4 and a few times 10^5 A, depending on the width of the bubble.

Shiokawa et al. (1997) have studied the braking of fast flows at the inner edge of the plasma sheet, where the tail magnetic field becomes dipolar. Two different processes contributed to the generation of FACs there. The first is the braking of the flow, leading to inertial currents. This led to a total disrupted current of about $7 \cdot 10^4$ A. The other process was due to the pile-up of magnetic flux where the flows

are braked. This resulted in a total current of about $1.2 \cdot 10^5$ A.

It is important to point out that the diversion of the tail current does not necessarily lead to FACs. It can also close locally in the tail by perpendicular currents. In addition, as discussed in the beginning of this chapter, the magnetosphere must be a generator if the FACs close in the ionosphere. This requires that

$$\mathbf{j} \cdot \mathbf{E} = -\mathbf{j} \cdot (\mathbf{u} \times \mathbf{B}) = \mathbf{u} \cdot (\mathbf{j} \times \mathbf{B}) = \mathbf{u} \cdot (\nabla_{\perp} p + \rho_m \frac{d}{dt} \mathbf{u}_{\perp}) < 0, \quad (3.2)$$

where the frozen-in approximation has been utilised. It can be seen that deceleration of the flow makes it a generator. Furthermore, *Birn and Hesse* (2005) have shown that the vortices at the flanks of the flux tube can be generators. This happens above and below the neutral sheet. There the vortex flows will get a component along the Z -axis towards the lobes leading to $\mathbf{u} \cdot \nabla_{\perp} p < 0$. Observations of such a vortex flow associated with a field aligned current is observed in Paper I at the flank of a depleted flux tube in the outer CPS.

3.2 Reconnection and Hall currents

So far the frozen-in approximation has been assumed to be valid. This is not adequate when the current sheet becomes so thin that it is comparable with the ion gyro radius. When this happens, the frozen-in approximation will be invalid for the ions. It can still be valid for the electrons, because of their smaller gyro radius. The gyro radius R , is proportional to the square root of the product of the mass and temperature for a thermal particle.

$$R = \sqrt{\frac{2k_B T m}{q^2 B^2}} \quad (3.3)$$

With a mass ratio of 1800 and a temperature ratio of 7 in the plasma sheet (*Baumjohann et al.*, 1989), the ions have about hundred times larger gyro radius than the electrons.

Figure 1 in paper III shows an illustration of the reconnection region. The ion diffusion region and the electron diffusion region are marked (not in actual scales). *Sonnerup* (1979) showed that the deviation of the ion velocity from the $\mathbf{E} \times \mathbf{B}$ drift in the ion diffusion region, gives rise to Hall currents. These currents are shown with dashed lines in the figure. The scale of the diffusion region perpendicular to the current sheet is given by the inertial length

$$\lambda = \sqrt{\frac{m}{\mu_0 n q^2}}. \quad (3.4)$$

The currents are equivalent with a quadrupolar signature in B_Y , which we have used to identify the reconnection region used to identify the reconnection region in Paper III.

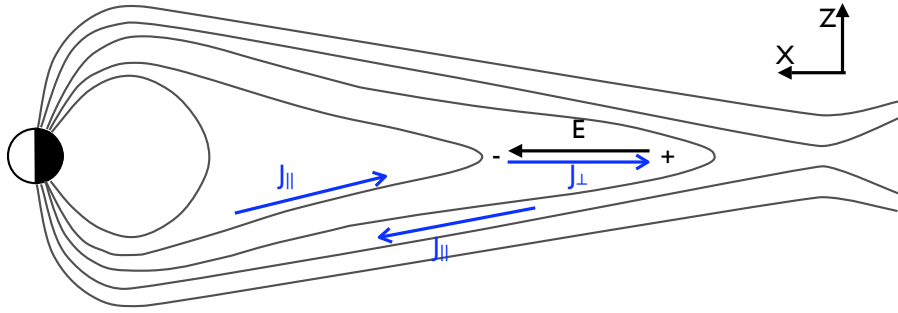


Fig. 3.2. A meridional current system.

Treumann et al. (2006) have shown that the divergence of the Hall currents in the ion diffusion region creates field aligned currents in and out of the reconnection region. In a Hall-MHD simulation of reconnection, *Yamada et al.* (2000) estimated the FACs to be of the order of 10^5 A. The Hall current system consists of FACs towards the X-line in the outflow regions and FACs away from the X-line in the inflow regions. In the inflow region there was a north-south electric field pointing towards the neutral sheet. Since this electric field is opposite of the Hall current, this forms a generator. The field aligned currents closing with the Hall currents are the topic for Paper II a and Paper IV.

Nakamura et al. (1998) used a 2D hybrid simulation code in which ions were treated as particles, while electrons were treated as a massless fluid. In their simulation electrons had higher outflow speed than the ions. This led to a current towards the X-line. In addition, they found that an opposite current was created at the leading front of the jet, where it interacted with the pre-existing plasma. This was due to the fact that electrons are slowed down faster than ions, because of their lower inertia.

There seems to be some controversy related to the scale of the ion diffusion region in the X -direction. *Nakamura et al.* (1998) found it to be about 10 ion inertial lengths ($10 \cdot 1000$ km for a lobe density of 0.05 cm^{-3}). In a particle-in-cell simulation *Shay et al.* (2007) showed that the outflowing electrons can form a jet where the electrons are decoupled from the magnetic field. The jet extended several tens of ion inertial lengths downstream from the X-line. However, *Nagai et al.* (2003) performed a 2-D full particle simulation of magnetic reconnection and found that the B_Y perturbation only existed near the boundary between the inflow and outflow regions called the separatrix layers.

Since the only prerequisite for the generation of Hall currents is that the ions become demagnetised, one can imagine that similar currents can exist without reconnection. For instance, during earthward convection of magnetic field lines, only electrons will follow the field lines if the current sheet becomes sufficiently thin. In fact, *Lui and Kamide* (2003) have proposed such a current generation mechanism during dipolarization in the near-Earth tail. They called it a meridional current

system. Figure 3.2 shows an illustration of this. The differential motion between ions and electrons creates both an earthward directed electric field and a tailward directed current. They estimated the total current strength to be of the order of 10^7 A.

Chapter 4

Observations

In the previous chapters we have shown that reconnection and fast flows are key elements for the earthward convection in the magnetotail. We will now continue to describe these phenomena from an observational point of view. However, a theoretical framework is required to interpret these observations. We will try to show how different models have led to radically different explanations of the same observation. The selection criteria in experimental studies are crucial for the results. The various criteria will therefore be carefully addressed.

Observations of fast flows are examined first. Then we present observations from the reconnection region. In Sect. 4.3 are statistical observations from the ionosphere and the magnetosphere shown, and a discussion of how these observations may relate to the FACs we have studied is given.

4.1 Fast flows

Two different models for the plasma sheet convection will be discussed first, and it is shown how the scientific results in the recent years have led to the dominating view today that bursty bulk flows are the major contributor to convection in the near-Earth plasma sheet. This is followed with a section where the earthward transport of magnetic flux is described in more depth. Section 4.1.3 describes the observations during fast flow events. Different interpretations of what the observations tell about the structure of the BBFs are presented. These interpretations are relevant for the flow can move earthward and how field aligned currents are produced, and serves as the basis for understanding the results reported in Paper I.

4.1.1 Transport of plasma and magnetic flux in the near-Earth plasma sheet

Baumjohann et al. (1990) studied the occurrence rate of fast flows in the plasma sheet for $-9 > X_{\text{GSM}} > -19 R_E$ and $|Y_{\text{GSM}}| < 10 R_E$. Plasma sheet samples

were distinguished from lobe samples by the requirement that the count rate in either the keV ion or the keV electron channels had to be above the background. Space craft charging effects were used to separate the PSBL from the CPS. At last, $B_{XY} \leq 15$ nT or $B_Z/B_{XY} > 0.5$ (in GSM) were used to identify the inner CPS. The remaining samples were from the outer CPS.

An important finding of *Baumjohann et al.* (1990) was that the occurrence rates of flows in excess of 400 km/s were 2.4%, 0.7%, and 4.0% for the inner CPS, outer CPS and PSBL, respectively. This indicated that the inner CPS was an important region for the earthward convection. A reason for the low occurrence rate in the outer CPS, might be that counter-streaming beams often are present there, so the bulk velocity is cancelled out. The high speed flows were very bursty in all the regions, with a majority lasting less than 10 s.

Based on these results, *Angelopoulos et al.* (1992, 1994) introduced the concept of a bursty bulk flow (BBF). They defined a flow burst as a sample with $V > 400$ km/s in the inner plasma sheet. A BBF was defined as a continuous series of samples with $V > 100$ km/s in the plasma sheet (inner and outer plasma sheet). 0.01 nPa was defined to be the boundary between the plasma sheet and the lobes. This value was chosen conservatively to avoid lobe samples in their study. Inner and outer plasma sheet were determined from plasma $\beta > 0.5$ and plasma $\beta < 0.5$, respectively (see Sect. 6.1 for a discussion of the use of plasma β as an identifier of plasma sheet regions). In addition, flow bursts separated by less than 10 min were defined to belong to the same BBF. This was done to avoid that short departures of the satellite from the flow channels should define the end of the BBF interval. Although this is a purely experimental definition, the acronym BBF has become common in use as a concept of fast convective flows in the CPS.

Angelopoulos et al. (1994) found that BBFs typically lasted for 100 to 2000 s, with an average duration of 550 s for $-10 > X > -22 R_E$. BBFs accounted for 60-100 % of the measured transport of mass, energy and northward flux in the region of maximum occurrence rate, which was tailward of $X \approx 15 R_E$ and around midnight. They noted that the duration could be underestimated, because of spatial variations in the flow causing the spacecraft to leave the flow before it has ended. In fact, using observations from three Cluster satellites *Cao et al.* (2006) found that the mean duration of a BBF was 1105 s. This also indicates that such flows are localised phenomena in the plasma sheet.

Paterson et al. (1998) disputed the results of *Angelopoulos et al.* (1994). Based on Geotail data they found that transverse earthward flows, $V_{\perp X}$, which exceeded 300 km/s, occurred in less than 0.1 % of the samples in the plasma sheet, where they defined the plasma sheet as the region where plasma $\beta > 0.1$. This showed that fast earthward transport perpendicular to the magnetic field was insignificant in the plasma sheet. They concluded that the concept of BBFs were a misinterpretation of the data, and that the data contained mostly field aligned beams. Field aligned beams are a part of the boundary layer model for magnetospheric convection. As described in Sect. 2.3 and shown in Fig. 2.4, particles are accelerated in the accel-

eration region in the distant tail, and then ejected earthward as field aligned beams (FABs). If there is a cross tail electric field, the FABs will convect slowly towards the neutral sheet as they move along the magnetic field. When they approach the strong magnetic field near the Earth, they will be reflected. An observer in the near-Earth tail will experience fast earthward FABs in the outermost layer of the PSBL. Deeper inside, there will be two counter-streaming beams. The tailward beam will be the one that already has been reflected. In the central plasma sheet (CPS), the beams merge to become a stagnant hot population. This model is well documented by observations (e.g. *Nakamura et al.*, 1992).

The criticism of BBFs was addressed by *Raj et al.* (2002). They investigated the distribution of 85 fast flow events, detected by the Wind satellite during 17 Wind passes through the plasma sheet, within 25 R_E from Earth. A single event was defined as a continuous period with flow speed above 250 km/s. The only restriction they set, was that the spacecraft should not be in the lobe immediately before it detected the flow. This may have excluded some cases.

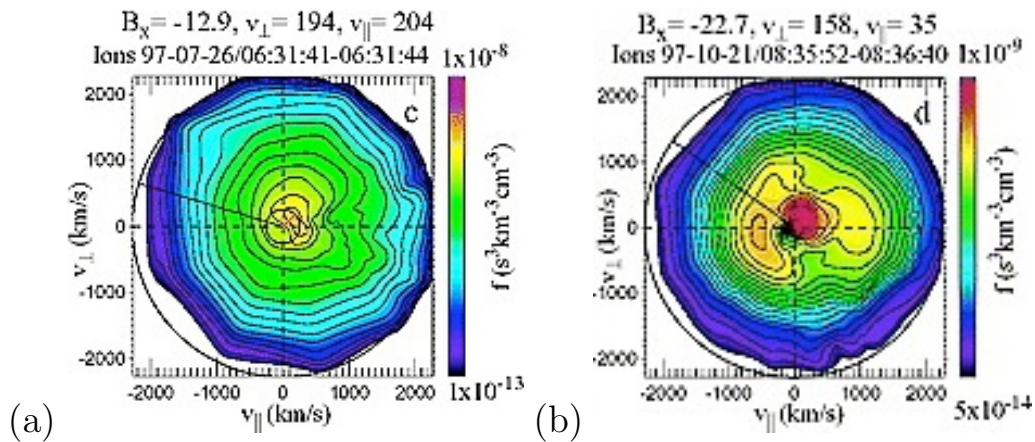


Fig. 4.1. a: A bulk flow distribution. b: A field-aligned beam distribution. The black line indicates the sunward direction. From *Raj et al.* (2002).

They found that all distributions could be one of two types: Bulk flows or field-aligned beams (FABs). Typical distributions of both types are shown in Fig. 4.1. Bulk flow distributions were characterised by symmetric populations displaced from zero. The FAB distributions had a low energy cut-off and were highly field aligned. In addition, another colder population could be present in the FAB distribution. It had the same $\mathbf{E} \times \mathbf{B}$ drift as the dominant distribution, but its parallel velocity was usually much smaller. In Fig. 4.1b the cold population is the dense red spot near the origin.

60 % of the fast flows were bulk flows. Bulk flows and FABs were primarily observed in the CPS and PSBL, respectively, but there was also a considerable region of overlap. In terms of the magnetic field, bulk flows were found for $|B_x| < 25$ nT,

while FABs were found for $|B_X| > 5$ nT. This criterion was used to exclude field aligned beams for the statistical study in Paper II. Bulk flows could have large parallel velocities and *Paterson et al.* (1998) could therefore have mistaken FABs with BBFs. The ratio between the parallel and perpendicular components was mainly dependent on the magnetic field elevation angle, defined as $\tan^{-1}(B_Z/B_{XY})$. The selection criteria of *Angelopoulos et al.* (1994) for flow bursts, would have included approximately 20 % FABs. No selection criteria based on moments of the distribution function could include all bulk flows and exclude all FABs. The optimal selection criteria were found to be $V_{\perp} > 250$ km/s and plasma $\beta_{XY} > 2$. Those excluded 95 % of the beams and included 60 % of the bulk flows.

4.1.2 Earthward boundary of fast flows

Both *Baumjohann et al.* (1990) and *Angelopoulos et al.* (1994) observed that the occurrence rate of earthward fast flows is decreasing rapidly earthward. *Shiokawa et al.* (1997) used the same data set and definition of the plasma sheet as *Baumjohann et al.* (1988, 1989) to study this phenomenon. They noticed that although the occurrence rate was decreasing, the magnitude of the flows did not decrease. This led them to suggest that the fast flows are halted abruptly at a clear boundary between the regions of the dipolar field and the tail-like field in the plasma sheet.

Schödel et al. (2001) chose another approach to study flux transport in the CPS. The CPS was defined as plasma $\beta > 0.5$. They defined a rapid flux transfer (RFT) event as a plasma flow which takes place in the CPS, with $v_{\perp} > v_{\parallel}$ and $E_H = V_H B_Z > 2$ mV/m, where $V_H = \sqrt{V_X^2 + V_Y^2}$. They used Geotail data from $-50 < X_{\text{AGSM}} < -10 R_E$. An electric field of 2 mV/m corresponds to a velocity of 400 km/s in a northward magnetic field of 5 nT. Furthermore, the potential drop across a $3 R_E$ wide flow channel would be ~ 40 kV, which is comparable to the potential drop across the polar cap in active periods (*Haaland et al.*, 2007). *Sergeev et al.* (2001) have also suggested that multiple flow channels can occur at different local times, giving rise to more rapid flux transport.

The right panel in Fig. 4.2 shows that the occurrence rate of earthward flows increases with the distance from the Earth. On the other hand, the left panel shows that the occurrence rate of rapid flux transport is almost constant for $-45 > X > -17.5 R_E$. It shows only a slight decrease of $\sim 30\%$ from $X = -17.5 R_E$ to $X = -12.5 R_E$. This indicates that fast flows are braked gradually as they are moving earthward into regions of stronger magnetic field.

Schödel et al. (2001) also defined a rapid convection event (RCE) as an analog to a BBF. It was defined similarly to a BBF, except that the flow limits of 100 and 400 km/s were replaced with flux transport limits (E_H) of 0.5 mV/m and 2 mV/m, respectively. Their estimates of total transport of mass and flux were in accordance with the results found earlier for BBFs by *Angelopoulos et al.* (1994), but were slightly lower. However, this was probably due to stricter selection criteria, as suggested by *Cao et al.* (2006). They found that the average duration of RCEs

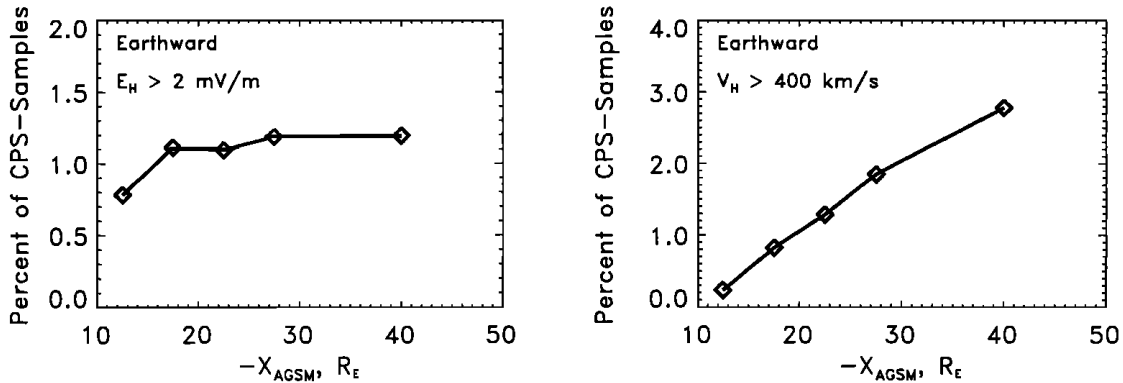


Fig. 4.2. The occurrence rates of RFT samples and fast flows in the CPS for $|Y_{\text{AGSM}}| < 10 R_E$. $E_H = V_H B_Z$ where $V_H = \sqrt{V_X^2 + V_Y^2}$. From *Schödel et al.* (2001).

was 445 s, which is much lower than for BBFs (1105 s). On the other hand, the number of RCEs was $\sim 50\%$ higher than the number of BBFs in their data set. Despite these discrepancies, there is reason to believe that RCEs and BBFs are the same phenomenon.

4.1.3 Structure of fast flows

The central plasma sheet is a very dynamic region, especially during fast flows. It is often difficult to separate between temporal and spatial variations. Superposed epoch analysis (SEA) is a statistical method to find an underlying pattern in time series. The method is carried out by using the average of all measurements observed at a particular time relative to a reference time. This is repeated for all relative times until an average time series (composite) is found. Given sufficient data, a common underlying pattern should theoretically emerge in the composite, while other noise in the data should disappear.

Figure 4.3 shows a SEA by *Ohtani et al.* (2004). They and many other researchers had noticed that the leading edge of BBFs often was characterised by increased B_Z . The reference time for the SEA was therefore chosen to be when B_Z increased most in a 4 minutes time interval centered at the start of the flow. The start of the flow was set to be when $V_{\perp X}$ exceeded 300 km/s and $\beta > 0.5$. They used Geotail data from $-31 < X_{\text{GSMA}} < -5 R_E$ and $|Y_{\text{GSMA}}| < 15 R_E$ for the analysis.

We will now describe different characteristics of observations during BBFs. Most of these features are shown in Fig. 4.3. The observations and their interpretations are summarised in Table 4.1. Some observations have more than one interpretation. The different interpretations will be described below.

Around $\Delta T_B = 0$, B_Z first decreases by ~ 1.5 nT for about 1.5 min, then increases with more than 5 nT in less than one minute and at last decreases gradually

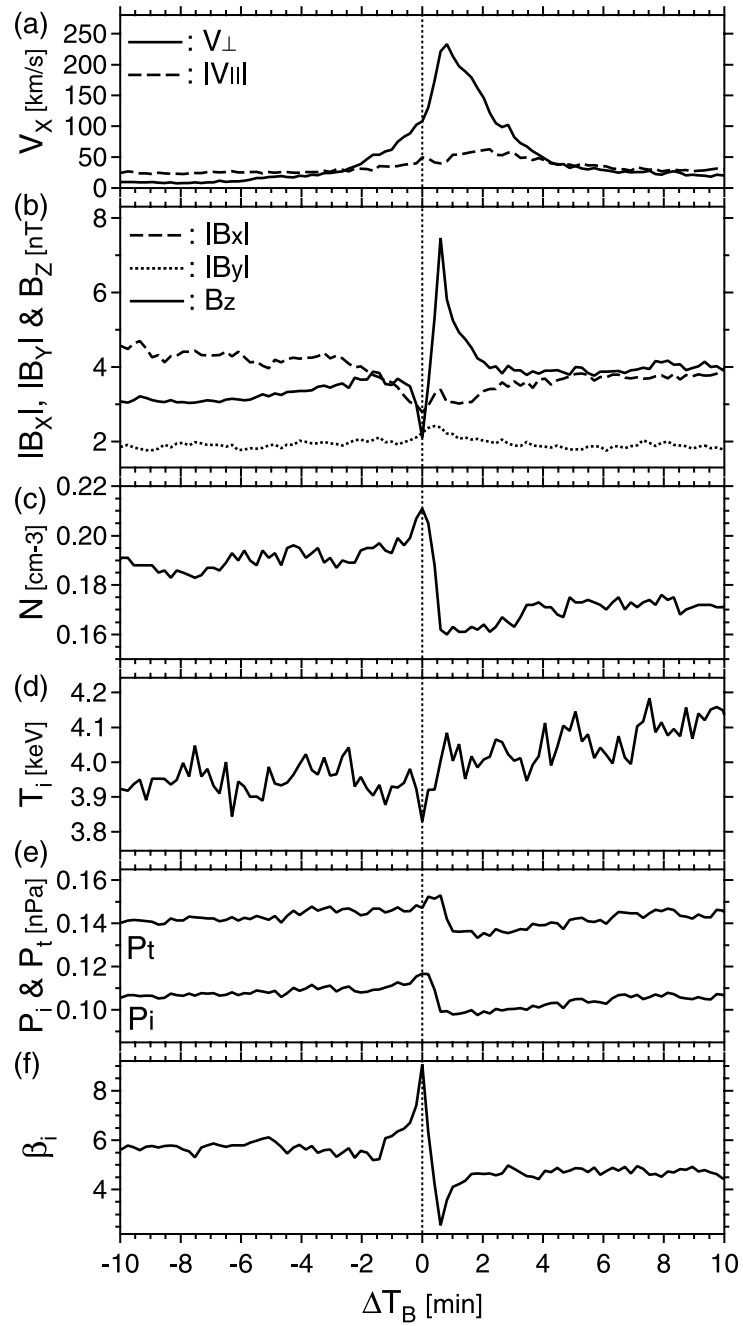


Fig. 4.3. Various magnetic field and plasma parameters superposed for 818 fast earthward flow events. The reference time T_{0B} is defined as the start of the 36 s interval where B_z shows largest increase. From *Ohtani et al. (2004)*.

Observation ($\Delta T_B/\text{min}$)	Interpretation
Gradual decrease of B_Z (-0.5)	Flux rope, NFTE, Interaction of BBF with surrounding plasma
Increased density (0.0)	Interaction of BBF with surrounding plasma
Rapid increase of B_Z (0.3)	Flux rope, NFTE, BBF boundary
Perturbation in $ B_Y $ (0.3)	Flux rope, Interaction of BBF with surrounding plasma
Flow shear in V_Y and/or V_Z (0.3)	Interaction of BBF with surrounding plasma
Gradual decrease of B_Z (1.0)	Flux rope, NFTE, Rear part of bubble
Increased B_Z and temperature, Decreased B_X and density (2.0)	Depleted flux tube, dipolarization

Table 4.1. Typical observations during BBFs. The numbers in parentheses refer to the approximate time (ΔT_B in Fig. 4.3) for the different features. See the text for details about the interpretations.

to about the level it had before the perturbation. This has been interpreted as a flux rope at the leading edge of the flow (Slavin *et al.*, 2003, and references therein). This scenario is illustrated in Fig. 4.4. Multiple X-lines are shown at different distances from the Earth. In the beginning all of them will reconnect closed field lines which will form flux ropes in the plasma sheet. The X-line which first starts to reconnect lobe field lines, will “push” all earlier produced flux ropes earthward or tailward. This can explain the bipolar signature in B_Z observed at the leading edge of the flow. A line current along the axis of the flux rope causes the the rapid increase in B_Z when the spacecraft crosses the center of the flux rope. The perturbation of B_Y is caused by an azimuthal component of the flux rope current.

Another explanation is that the bipolar signature is due to a night side flux transfer event (NFTE) (Sergeev *et al.*, 1992, see also Sharma *et al.* (2008) Sect. 2.5). An illustration of this is shown in Fig 4.5. An X-line is situated to the right of

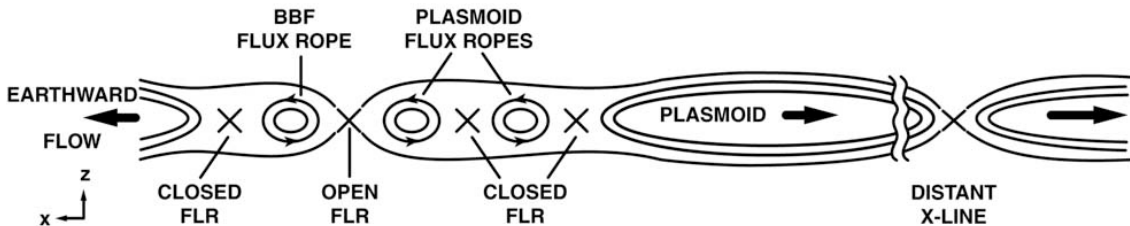


Fig. 4.4. Schematic description of the formation of earthward and tailward moving flux ropes as a result of simultaneous field line reconnection (FLR) at multiple neutral lines in the $X - Z$ plane. From Slavin *et al.* (2003).

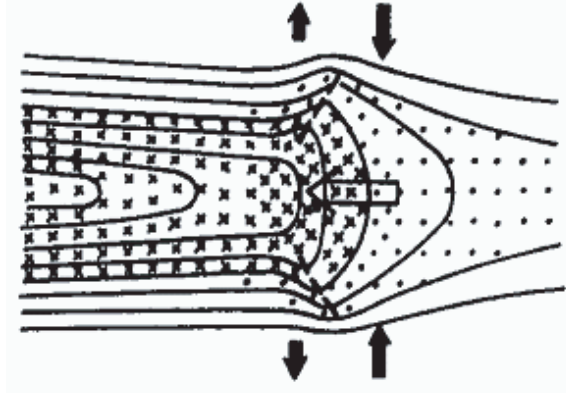


Fig. 4.5. Configuration of a NFTE in the XZ -plane. The plasma is flowing to the left. The up and down arrows illustrate how the magnetic field is perturbed above and below the leading edge of the flow. From *Sergeev et al.* (1992).

this figure and the plasma is flowing to the left. The dipolar field lines between the arrows, represent the leading part of the flow where B_Z has increased. This creates a bulge in the magnetic field north and south of the flow. This model explains better the asymmetry in the bipolar signature in Fig. 4.3b. Since B_Z never decreases below zero, it is inconsistent with the closed magnetic loops in a flux rope.

By using multi-spacecraft measurements from Cluster, *Nakamura et al.* (2004b) found the spatial dimensions of BBFs. They had a dawn-dusk width of 2-3 R_E and a scale of 1.5-2 R_E in the north-south direction. If the earthward moving flux tube in Fig. 2.3 has to push all flux tubes ahead earthward, it would quickly be braked because of the pressure build-up. However, the narrow width of the flux tube allows it to penetrate into the pre-existing plasma, by pushing it aside. This scenario is depicted in Fig. 4.6 from *Sergeev et al.* (1996). It illustrates the cross section of the front part of a bubble as it moves earthward. The curved arrows emanating from the bubble represent plasma that is pushed aside. *Sergeev et al.* (1996) studied the orientation of the fast flows by estimating the normal when the satellite crossed the boundary of the flux tubes. The normals often had large Y and/or Z components indicating narrow flow channels in the plasma sheet. The effects are flow shear and magnetic twisting (*Nakamura et al.*, 2005). This is manifested as perturbations in B_Y and V_Y near the neutral sheet as shown in Fig. 4.6. In the outer CPS B_Z and V_Z can be perturbed as well, as shown in paper I. This gives a similar signature as a flux rope or a NFTE. There is also an increase in the density just ahead of the flux tube, indicating compression of the plasma.

Many of the features predicted from the theory of depleted flux tubes described in Sect. 2.4.1, are reproduced in Fig. 4.3. By comparing B_Z and the temperature before and after the initial perturbation of the magnetic field, it appears that their values have increased, while the density and B_X have decreased (*Sergeev et al.*, 1996; *Nakamura et al.*, 2005). The larger B_Z inside the flux tube adds to the twisting of

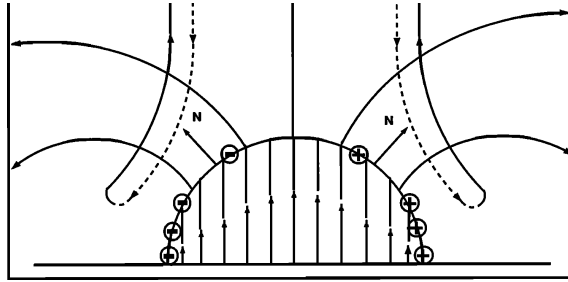


Fig. 4.6. Schematic view (from the north) of the front of an earthward moving bubble. The curved arrows radially out of the bubble illustrates how plasma is “pushed” aside. This bends the magnetic field lines ahead of the bubble. From *Sergeev et al.* (1996).

the magnetic field at the BBF boundary, which gives rise to field aligned currents.

The decrease of B_X is interpreted as being due to expansion of the current sheet. But fast flows are also known to occur during current sheet thinning. *Nakamura et al.* (2002) observed that the current sheet thickness decreased from 5000 to 400 km when a fast flow started. They interpreted the thinning as an effect of the spacecraft being close to the X-line when the flow started. The current sheet also became bifurcated which also has been observed in the outflow region (*Asano et al.*, 2004). This will be described in the next section.

4.2 Near-Earth reconnection

The near-Earth reconnection region and the surrounding area have been studied in detail by *Asano et al.* (2004). They used measurements from Geotail in the period 1 May 1995 - 10 June 1997. To identify reconnection candidates they first looked for reversals from (1) tailward flow with negative B_Z to (2) earthward flow with positive B_Z , where the time between (1) and (2) were less than 1 h. Both the tailward and the earthward flows had to exceed 300 km/s. In addition, to identify the reconnection region they used the following criteria: (I) $n_i < 0.1 \text{ cm}^{-3}$ and (II) $|V_{eX} - V_{iX}| > 500 \text{ km/s}$. (I) and (II) had to occur within 15 min before the end of the tailward (after the start of the earthward) flow. Criterion II was to make sure that Geotail was in the ion diffusion region. They found 23 events mainly between 20 and 30 R_E . This agrees well with earlier studies of the flow reversal region (*Nagai and Machida*, 1998; *Nagai et al.*, 1998, and references therein).

Figure 4.7 shows a sketch that summarises many of their observations in the reconnection region. As described in detail in Sect. 3.2, Hall currents are set up in the ion diffusion region due to the different velocity of the ion and electron. These currents are difficult to observe, but many studies have observed the field aligned currents which close with them. *Nagai et al.* (1998) observed high energy ($> 10 \text{ keV}$)

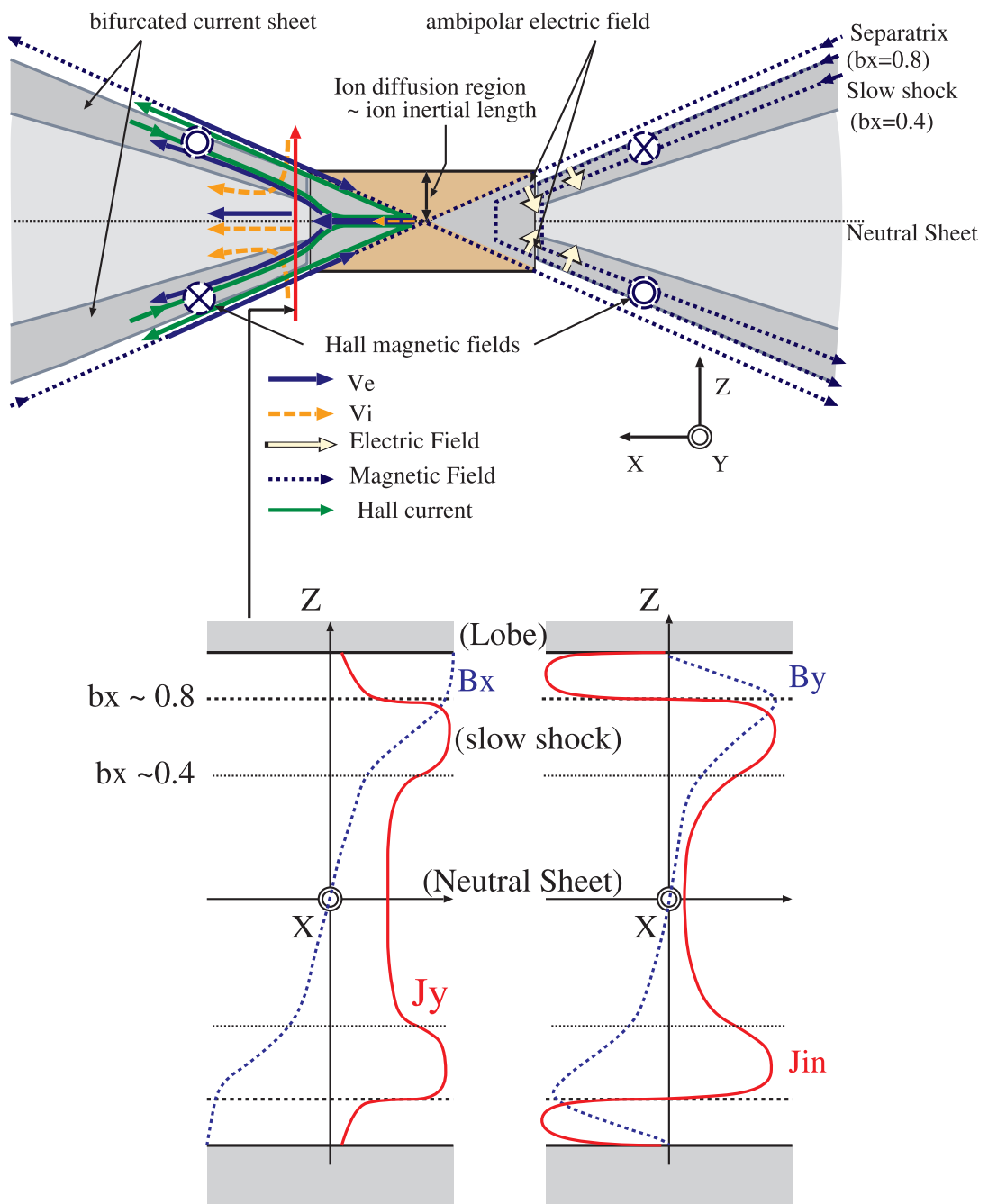


Fig. 4.7. Overview of the reconnection region. From *Asano et al.* (2004).

field aligned electrons away from the X-line and medium energy (~ 3 keV) field aligned electrons into the X-line close to the separatrix. This was interpreted as acceleration of electrons in the reconnection region. *Nagai et al.* (2001) found that the medium energy electrons can carry a current out of the reconnection region. *Nagai et al.* (2003) reinvestigated these events based on better calibrated data. They calculated the current densities only in the outer plasma sheet, when the magnetic field was stable and when counterstreaming electrons were observed. They found a thin double sheet current structure with current into the X-line for higher electron temperatures than for currents out from the X-line. This was consistent with their simulation (Sect. 3.2).

Another way to identify the Hall current system is by the quadrupolar pattern it should produce in B_Y (see also Fig. 1 in paper II). A comprehensive statistical study has been done by *Ueno et al.* (2003) based on Geotail data between 1993-2001 in the region $0 > X_{\text{GSM}} > -50 R_E$. They searched for the following change between one minute average samples: B_Z and V_X change from negative (positive) to positive (negative) together with an increase (decrease) and decrease (increase) of the density of earthward and tailward flowing ions, respectively. The last criterion was to make sure that both earthward and tailward flowing ions had the same source. They found 4022 flow reversal events. The mean B_Y variation was identified as a quadrupolar structure with a magnitude of about 1% of the lobe magnetic field, B_L . For $|B_Z| > 0.1B_L$, the magnitude increased to 5% of B_L . B_Z can be used as a measure of the distance from the X-line, since the field is more dipolar away from the X-line. Their interpretation of the dependence between B_Y and B_Z was that the Hall current system was fully developed only outside the reconnection region.

In the previous section it was noted that BBFs can be observed both in thick and thin current sheets, and that this could be an indication of the distance from the X-line. *Asano et al.* (2004) found that the current sheet width increased from about 3000 km a few minutes after the flow reversal to about 10000 km 30 min after the flow reversal. The lower left panel in Fig. 4.7 shows how the cross tail current (red line) is distributed in the current sheet. The current density is strongest above and below the neutral sheet ($Z = 0$). This is called a bifurcated current sheet. In the lower right panel of Fig. 4.7 the X -component of the current density near the reconnection region is shown (red line). Positive values corresponds to a current into the X-line, while negative values mean that the current is directed out of the X-line. These currents are most likely part of the Hall current system, as illustrated with the green arrows in and out of the X-line in Fig. 4.7.

By comparing the left and right panels in Fig. 4.7, it can be seen that the inward current peaks where the current sheet is most bifurcated, indicating a connection between these phenomena. This can be explained in the following way. In the ion diffusion region, the demagnetised ions do not follow the magnetic field lines towards the X-line. This creates a southward (northward) electric field between the CPS and the northern (southern) PSBL. *Asano et al.* (2004) observed that electrons were moving downward just where the current sheet was most bifurcated.

By estimating the electric field from the frozen-in approximation, which should hold very well for electrons, they obtained a north-south electric field E_{ns} of about 5-7 mV/m. This exceeded E_Y by a factor 2-3. This electric field is easiest to explain by considering that the electric field in the ion diffusion region maps out of the reconnection region along the magnetic field lines. The current of the dawnward drifting electrons totally dominated over the ion currents in the outer plasma sheet.

These results showed that the demagnetisation of the ions both results in field aligned currents and a north-south electric field which can be detected outside the the reconnection region. *Asano et al.* (2004) also found that the inward and outward currents were detected closer to the lobes for higher values of B_Z . This support that the inward and outward currents are field aligned, since the field lines have a component perpendicular to the current sheet.

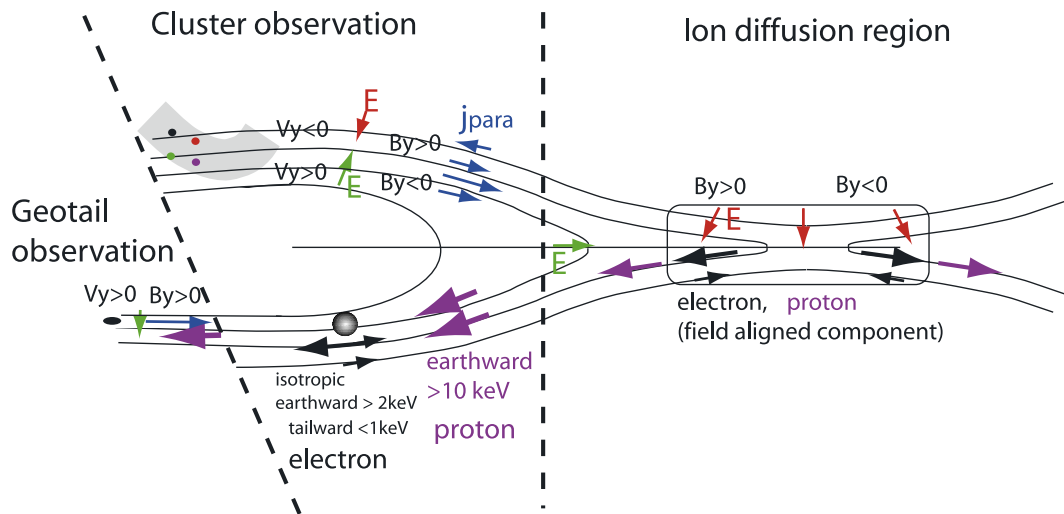


Fig. 4.8. An illustration of how observations in the PSBL may relate to the reconnection region. From *Nakamura et al.* (2004a).

Also observations remote from the reconnection have been reported, which can be explained in terms of the Hall current system. Interpretations of measurements from Cluster and Geotail by *Nakamura et al.* (2004a) are shown in Fig. 4.8. They observed dawnward velocity at the boundary between the PSBL and the northern lobe and duskward velocity further into the plasma sheet. They proposed that the dawnward velocity could be caused by a southward electric field from a reconnection cite. As mentioned in Sect. 3.2, the simulation by *Nakamura et al.* (1998) showed that electrons are slowed down faster near the leading edge of the reconnection jet. This may cause a tailward electric field as shown with the green arrow in Fig. 4.8. Mapped out to the outer CPS in the northern hemisphere this electric field will be northward. This can explain the observed duskward velocity. Furthermore, they observed field aligned currents close to the boundary between the lobe and the

plasma sheet with earthward current at the lobe side and tailward current just inside the boundary. The downward current away from the X-line was observed to be less than 1000 km thick, while the current in the opposite direction was much thicker. They confirmed that the downward current region is comparable to or smaller than the ion inertia length as expected if the current comes from the ion diffusion region.

The idea that the Hall currents can give rise to field aligned currents, motivated the statistical study in Paper II. By using fast flows in the neutral sheet to identify reconnection, we investigated B_Y perturbations to check if the Hall current system is reproduced away from the reconnection region. In Paper IV observations from the plasma sheet and from the ionosphere were compared to examine whether the Hall current system can close in the ionosphere.

4.3 Field aligned currents in the ionosphere and the magnetotail compared

Two types of field aligned current (FAC) systems are often associated with bursty bulk flows (BBFs) and reconnection in the magnetotail. The first is the localised current wedge created by the sheared magnetic field at the flanks of a BBF. The second is the Hall current system from an X-line. We will now discuss how these currents may be related to field aligned currents observed in the ionosphere.

Iijima and Potemra (1976) used the magnetometer on-board Triad to investigate FACs in the auroral zone. Figure 4.9 shows the resulting distribution as a function of invariant latitude and magnetic local time for disturbed geomagnetic conditions

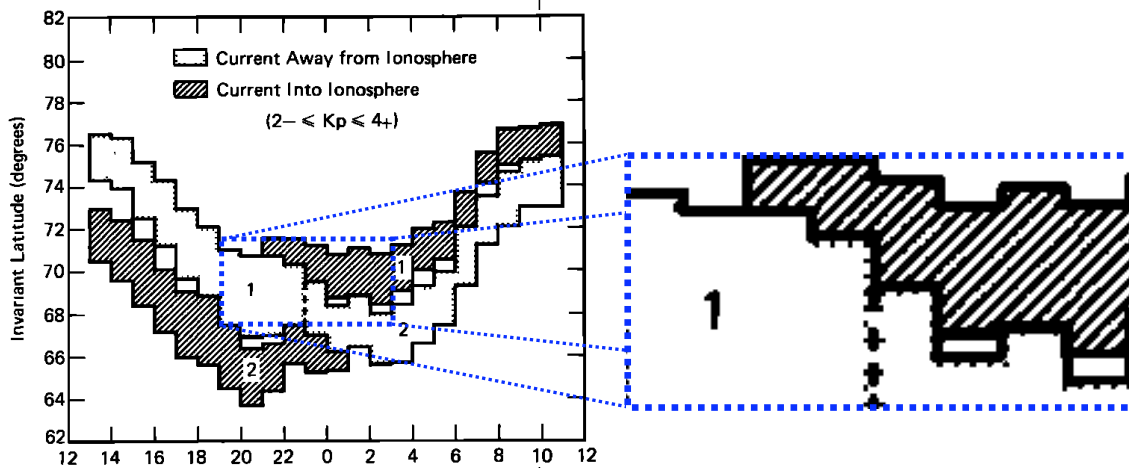


Fig. 4.9. Left: Spatial distribution of large scale field aligned currents during disturbed geomagnetic conditions ($2- \leq Kp \leq 4+$). Region 1 and region 2 currents are marked with corresponding labels. Right: A close-up on the region around midnight closest to the polar cap. From *Iijima and Potemra (1976)*.

($2- \leq Kp \leq 4+$). The Kp index is a measure of the disturbance of the ground magnetic field at mid latitudes. 90 degrees latitude corresponds to the magnetic dipole pole. *Iijima and Potemra (1976)* divided the FACs into two groups according to the latitude they were observed. The northernmost FACs observed at the poleward side of the auroral oval, were called region 1 currents, while the southernmost FACs were called region 2 currents and were observed at the equatorward side of the auroral oval.

The region 1 current on the evening, morning and dayside is related to the interaction between the magnetosphere and the solar wind at the magnetopause, and is an almost permanent phenomenon. The region 2 current in the same local times is related to the partial ring current in the inner magnetosphere. We will not elaborate on these processes and refer to (*Brekke, 1997*) for further details. The area we will concentrate on is the region around midnight, closest to the polar cap shown in the close-up in Fig. 4.9.

Ohtani et al. (1988) have done a statistical study of field-aligned currents in the PSBL. They presented data earthward of $20 R_E$. Based on the average position of the near-Earth X-line between $X = 20 R_E$ and $X = 30 R_E$, one can infer that most of the results are earthward of the reconnection region. The distribution as a function of local time is shown in Fig. 4.10.

Interestingly, one sees a similar dawn dusk asymmetry in Fig. 4.9 with more tailward current at the morning side and mainly earthward current at the evening side. How can this be explained in terms of the FAC current mechanisms described in this chapter? A BBF in the magnetotail is associated with a current wedge as illustrated in Fig. 3.1 with earthward current at the dawn flank and tailward current

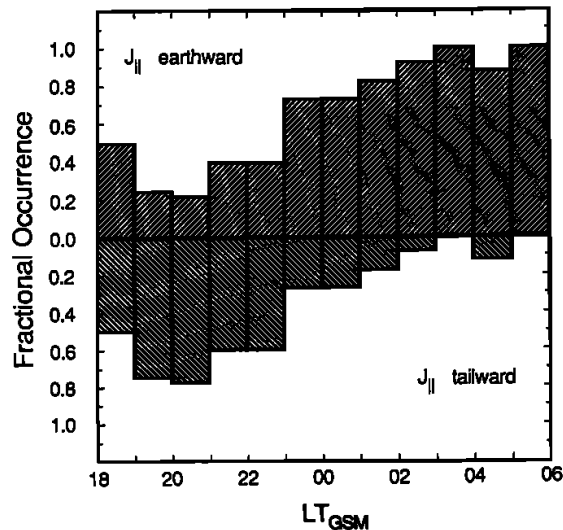


Fig. 4.10. Fractional occurrence of field aligned currents as a function of local time. The negative bars correspond to tailward currents. From *Ohtani et al. (1988)*.

at the dusk flank. This may explain the dawn dusk asymmetry. Reconnection is the mechanism which is likely to produce the BBF. But reconnection is also associated with the Hall current system with earthward current close to the lobe and tailward current closer to the neutral sheet. In a statistical distribution like Fig. 4.9 these two current systems will be superposed in the average pattern. This may explain the diagonal demarcation line between upward and downward currents in the ionosphere in the close-up in Fig. 4.9.

Chapter 5

Cluster

The main data sets that are analysed in this thesis are obtained by the Cluster spacecraft. We have also used data from other instruments and networks. They include the *International Monitor for Geomagnetic Effects* (IMAGE) magnetometer network, the *Imager for Magnetopause-to-Auroral Global Exploration* (IMAGE) satellite, the *Defense Meteorological Satellite Program* (DMSP) satellite and the *Polar* satellite.

On June 4 1996, Cluster was launched, but unfortunately the rocket exploded 30 s after lift-off (*Daly, 2002*). It was soon decided to rebuild the four spacecraft as the Cluster-II mission. Although the new mission was somewhat different from the original, one normally refers to it as Cluster. Cluster II was launched in two stages, on July 16 and August 9 2000 (*Escoubet et al., 2001*). The scientific objective was to study three dimensional structures in the magnetopause, the polar cusps, the magnetotail and the auroral zones. With a polar orbit of 4×19.6 Earth radii, they are ideally positioned to study the area just earthward of where near-Earth reconnection normally takes place; an important area to study in order to understand the transport of plasma and magnetic flux through the tail.

Cluster is a unique mission in the sense that it consists of four identically designed spacecraft. Their actual names are Rumba, Salsa, Samba and Tango, but are usually called C1, C2, C3 and C4. Each spacecraft can only measure physical quantities in-situ, but by using the difference in the measurements between the satellites, spatial derivatives can be estimated. Figure 5.2 shows how the separation between the spacecraft has varied. The ideal separation between the spacecraft depends on the spatial scale of the structure one wants to analyse. Data from primarily 2001 and 2002 have been used in this thesis. During these years the separation was ~ 2000 km and ~ 4000 km, respectively. This is larger than the gyro-radii of charged particles in the plasma sheet, and thus, it is large enough to use as fluid approach.

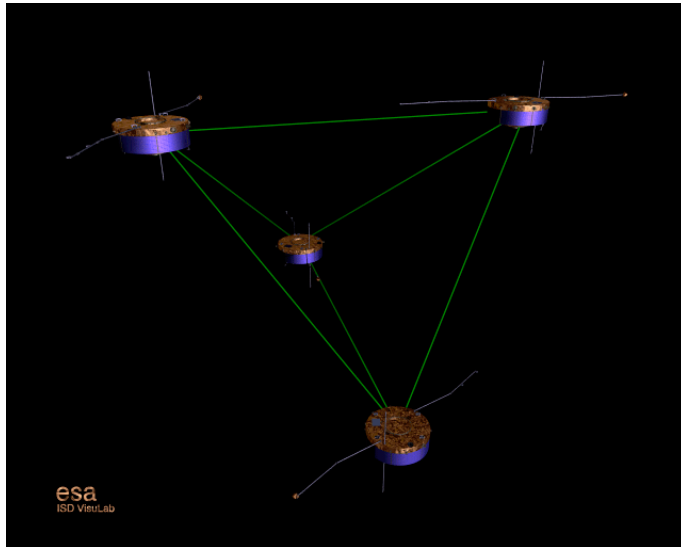


Fig. 5.1. Cluster consists of four spacecraft. [© European Space Agency]

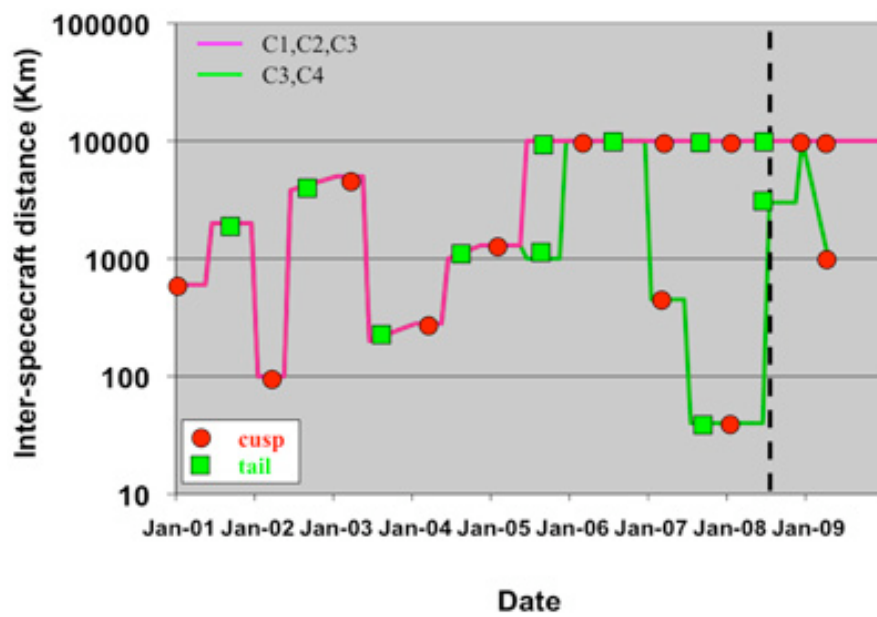


Fig. 5.2. Distance between the Cluster spacecraft while they have been in orbit. [© European Space Agency]

5.1 Data products

The data for the studies are from the fluxgate magnetometer (FGM) experiment (*Balogh et al.*, 2001) and the Cluster Ion Spectrometry (CIS) (*Rème et al.*, 2001). Magnetic field data with 4 or 0.2 seconds resolution from all four spacecraft have been used. The CIS instrument on C2 is not operational.

CIS is a package which consist of two different instruments. One is the Hot Ion Analyser (HIA), and the other is the time-of-flight ion Composition Distribution Function (CODIF). HIA only measures the energy per charge of particles, while CODIF also can determine the mass per charge. Since all the typical ions Cluster measures have different mass per charge, also the mass can be determined. In my master thesis (*Snekvik*, 2005) I found that HIA do not cover the lowest particle energies, so that the particle densities have a tendency to be underestimated. CODIF has therefore been used when possible, However, on C3 HIA has been used because CODIF is not working properly [B. Klecker, private communication, 2004].

Instruments such as HIA and CODIF measures the particle flux as a function of energy and solid angle relative to the spin axis of the satellite. The differential flux is defined as

$$j(t, \Omega, K) = \frac{dN}{dA dt d\Omega dK} \quad , \quad (5.1)$$

where dN is the number of particles with energy between K and $K + dK$, coming from a direction between (θ, ψ) and $(\theta + d\theta, \psi + d\psi)$, crossing an area dA , in the time interval from t to $t + dt$. The solid angle interval is defined as $d\Omega = \sin\theta d\psi d\theta$. The relation between the differential flux and the phase space density is:

$$j = \frac{v^2}{m} f \quad (5.2)$$

From the phase space density, fluid parameters such as velocity and pressure can be obtained from moments of f .

In practice, the particle count rates measured by the instrument are not equal to the real number of particles, it depends on the efficiency of the detectors. To estimate the real fluxes the data must be calibrated. Data which have been calibrated on-board the satellites, have a resolution of four seconds, but are usually of lower quality than ground calibrated data. For our studies only ground calibrated data have been used. They have a resolution of eight seconds for CODIF and 12 seconds for HIA.

Chapter 6

Single and multi spacecraft analysis methods

In the case of in-situ measurements it is necessary to know where the satellites are and how they are oriented relative to the structures they observe. This is often equivalent to reconstructing the topology of the structures. The simplest approach is to use the satellite position as a first approximation of where the satellites are. This is often done in statistical papers to set an initial limitation on the region of interest. However, since magnetospheric structures are very dynamic, this is not sufficient. More detailed information can be obtained by analysing the satellite measurements. The methods we have used will be described below and are summarised in Table 6.1.

Many observations in the magnetotail are interpreted as being due to magnetic reconnection. As explained in more detail in Sect. 4.2, tailward and earthward flows, northward and southward B_Z and dawnward and duskward perturbations in B_Y can be used to determine where the spacecraft are located relative to the X-line.

When observations from the ionosphere and the magnetotail have been compared, it has been necessary to identify where the field lines at the Cluster location end up in the ionosphere. The Tsyganenko models have been used for this in paper III and IV.

As all our studies have been from the plasma sheet, it has been necessary to identify where the spacecraft are located relative to the current sheet. By assuming that the current sheet consists of a unidirectional current, B_X will increase monotonically when crossing through the current sheet from the southern lobe to the northern lobe. A measure of location in the current sheet is therefore B_X itself, or B_X normalised with the lobe magnetic field $B_n = B_X/B_L$. The first four methods below are all related to the current sheet.

Method	Purpose	Papers
Spacecraft position	Rough determination of the magnetospheric regions	II, III
Flow direction and magnetic field orientation	Determine position relative to an X-line	II, III, IV
Tsyganenko models	Mapping from magnetosphere to ionosphere	III, IV
Plasma beta	Determine regions within the plasma sheet	I, II
Normalise magnetic field in current sheet with lobe magnetic field	Determine position in the current sheet	IV
Harris current sheet fit of magnetic field	Determine position in the current sheet	II
Linear gradient estimation from four spacecraft data	Reconstruction of current sheet structures	IV
Maximum variance analysis	Determine main magnetic field direction in a unidirectional current sheet	II, III, IV
Rank-2 least square approximation of magnetic field	Find normal of a TD discontinuity	I
Dehoffman-Teller Analysis	Find the velocity of structures	I
Cluster surface crossing	Determine local geometry of a surface	I

Table 6.1. Methods used to determine the position and orientation of Cluster relative to magnetotail structures.

6.1 Plasma β

In the statistical studies by *Baumjohann et al.* (1988, 1989), it was found that plasma β is the quantity which shows largest variation across the plasma sheet. Plasma β is the ratio between the thermal pressure and the magnetic pressure. Typical values for plasma beta were 0.02, 0.05, 0.3, 3 and 30 in the outer and inner PSBL, the outer and inner CPS and the neutral sheet (NS), respectively.

There are different ways to calculate plasma β . If temporal variations and the inertial and curvature terms in the MHD momentum equation are small, there will be pressure balance between the lobes and the CPS:

$$p_{\perp} + \frac{B^2}{2\mu_0} = \frac{B_L^2}{2\mu_0} \Rightarrow \beta + 1 = \frac{B_L^2}{B^2}. \quad (6.1)$$

Accordingly, if the pressure is anisotropic one should use the perpendicular pressure. Furthermore, if one assumes that typical scale lengths in the plasma sheet plane are much larger than along its normal (e.g. *Birn, 1987*), it can be shown that plasma

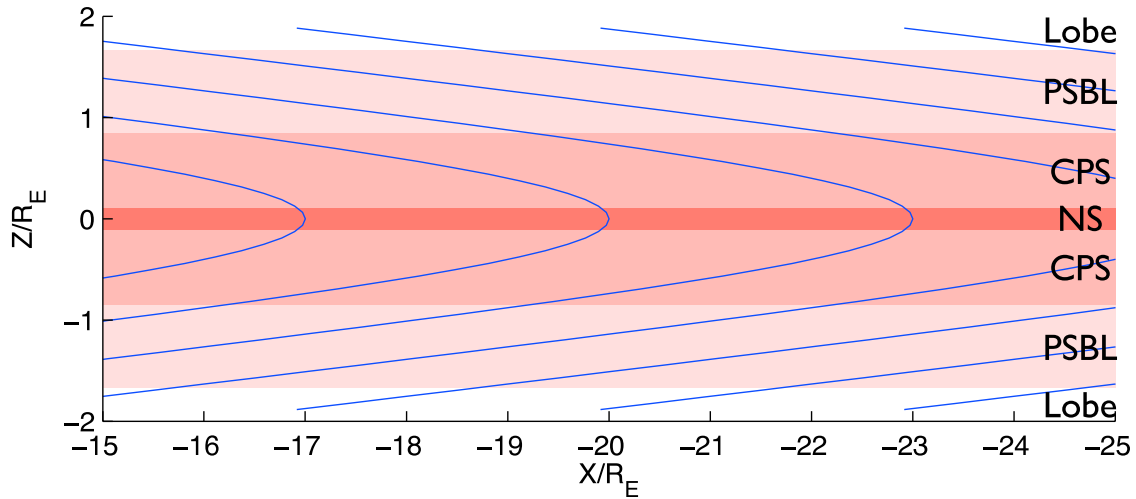


Fig. 6.1. A Harris current sheet with $L = 4000$ km, $B_Z = 3$ nT and $B_L = 25$ nT. The neutral sheet (NS), central plasma sheet (CPS), plasma sheet boundary layer (PSBL) and the lobes are shown, based on typical values of plasma β from (*Baumjohann et al.*, 1988, 1989).

β has largest variation perpendicular to the current sheet. In many cases it is not reasonable to assume that all of the components of the magnetic field are dependent on the distance from the neutral sheet. E. g. the B_Z component. It may be more sensible to use only the X and Y components of the magnetic field.

In spite of the assumption mentioned above, plasma β appears to be a quite robust parameter also during fast flows. *Raj et al.* (2002) found that plasma β_{XY} was the best parameter to distinguish between different types of flows. See also Sect. 4.1.1.

6.2 Harris current sheet

One can also fit the magnetic field to a Harris sheet model (*Harris*, 1962), where B_X is given by

$$B_X(Z = z) = B_L \tanh\left(\frac{z - z_0}{L}\right), \quad (6.2)$$

where z_0 is the center of the current sheet and L is its half thickness. An example of a Harris current sheet is shown in Fig. 6.1 using $\beta > 30$ for the NS, $0.3 > \beta > 30$ for the CPS and $0.02 > \beta > 0.3$ for the PSBL. The relation between plasma beta and Z is

$$\beta = \frac{1}{(\tanh(Z/L))^2} - 1, \quad (6.3)$$

when only B_X is used for the magnetic pressure. The advantage of using a current sheet model is that one can estimate the thickness of structures in real length units. How accurate these estimates are, will depend on how well the current sheet is approximated by this model. It is known that the current sheet often deviates from this model during reconnection and fast flows (e.g. *Asano et al.*, 2004).

6.3 Reconstruction of the current sheet

Another method we have used is based on the current sheet reconstruction model described by *Runov et al.* (2005). It utilises the spatial gradient estimation technique for four or more spacecraft (*Harvey*, 1998) and can be used in time intervals when Cluster crosses the current sheet. For each set of samples from the four spacecraft, a spatial derivative of B_X with respect to Z is estimated. This value is assigned to B_X in the spacecraft barycenter (the average position of the spacecraft). When this is repeated for all samples in the time interval, an empirical relation $Z(B_X)$ can be derived from

$$Z(B_X) = \int_{B_X=0}^{B_X} \frac{dB_X}{B'_X(Z)}. \quad (6.4)$$

This method is based on the assumption that the current sheet structures do not change much during the time interval. Apart from that, it is better than using a current sheet model, since no assumptions about the current sheet structure is required. However, the need for a current sheet crossing greatly reduces its usability.

6.4 Current sheet orientation

Many methods to obtain the current sheet orientation have been discussed in the literature (e.g. *Sergeev et al.*, 2006). Here, the discussion will be restricted to the one method we have utilised.

In paper II and IV we estimated field aligned currents from perturbations of B_Y , and in paper III we used B_Y to identify the reconnection region. For these purposes it was very important that the main magnetic field component was well determined. Otherwise, the cross tail current would influence the estimations of the FACs. To determine this direction, we performed variance analyses of the magnetic field during current sheet crossings. That involves finding the unique coordinate system where the magnetic field components are uncorrelated, i.e., the principal components of the magnetic field. In a current sheet carrying a unidirectional current, one can find the maximum variance direction under the assumption that the variance of the first principal component is much larger than the variance of the other two, which are due to noise (*Khrabrov and Sonnerup*, 1998b).

6.5 Boundary normal

When the spacecraft cross a tangential discontinuity, the normal can be found by a rank-2 least square approximation of the magnetic field. That means to find the orientation of the plane which gives the best two dimensional approximation of the magnetic field. This method was first used by *Siscoe et al.* (1968) and has been more thoroughly explained in Sect. 3.2 paper I.

6.6 deHoffmann-Teller analysis

When a three dimensional structure like a flux tube or a flux rope passes the spacecraft, large variation in the velocity and magnetic field will be measured. It can be difficult to determine the frame of reference of the structure. In a frame co-moving with the structure the time derivative of the magnetic field should be small (ideally zero). Based on Faraday's law, such a frame can be found by minimising the electric field by a deHoffmann-Teller Analysis (*Khrabrov and Sonnerup*, 1998a). If $-\mathbf{v} \times \mathbf{B}$ is used as a proxy for the electric field, the deHoffmann-Teller velocity, \mathbf{V} , can be found by minimising

$$D(\mathbf{V}) = \frac{1}{N} \sum_{i=1}^N |(\mathbf{v}_i - \mathbf{V}) \times \mathbf{B}_i|^2, \quad (6.5)$$

with respect to \mathbf{V} , where the sum is over all the measurements.

6.7 Curved boundaries

By using the boundary normals and the deHoffmann-Teller velocity, it is possible to reconstruct the curved surface of a structure passing the spacecraft. This method is based on a paper by *Mottez and Chanteur* (1994). A normal section of a surface at a regular point S is the intersection of the surface with a plane containing the normal vector. The two normal sections containing the two principal curvatures kp_1 and kp_2 are orthogonal with angles α_0 and $\alpha_0 + \pi/2$ in the plane tangential to the surface. The curvature k of a normal section is related to the principal curvatures by the Euler formula

$$k = \frac{kp_1 - kp_2}{2} \cos(2(\alpha - \alpha_0)) + \frac{kp_1 + kp_2}{2}. \quad (6.6)$$

The curvature is equal to the curvature radius inverse. An example of a surface is shown in Fig. 6.2. Let t_{i1} be the relative time when satellite i crosses the surface. The point where the satellite crosses the surface will then be given as $\mathbf{r}_i = \mathbf{r}_i(t = 0) - \mathbf{V}t_{i1}$ in a frame co-moving with the structure. By repeating this for all four spacecraft, we

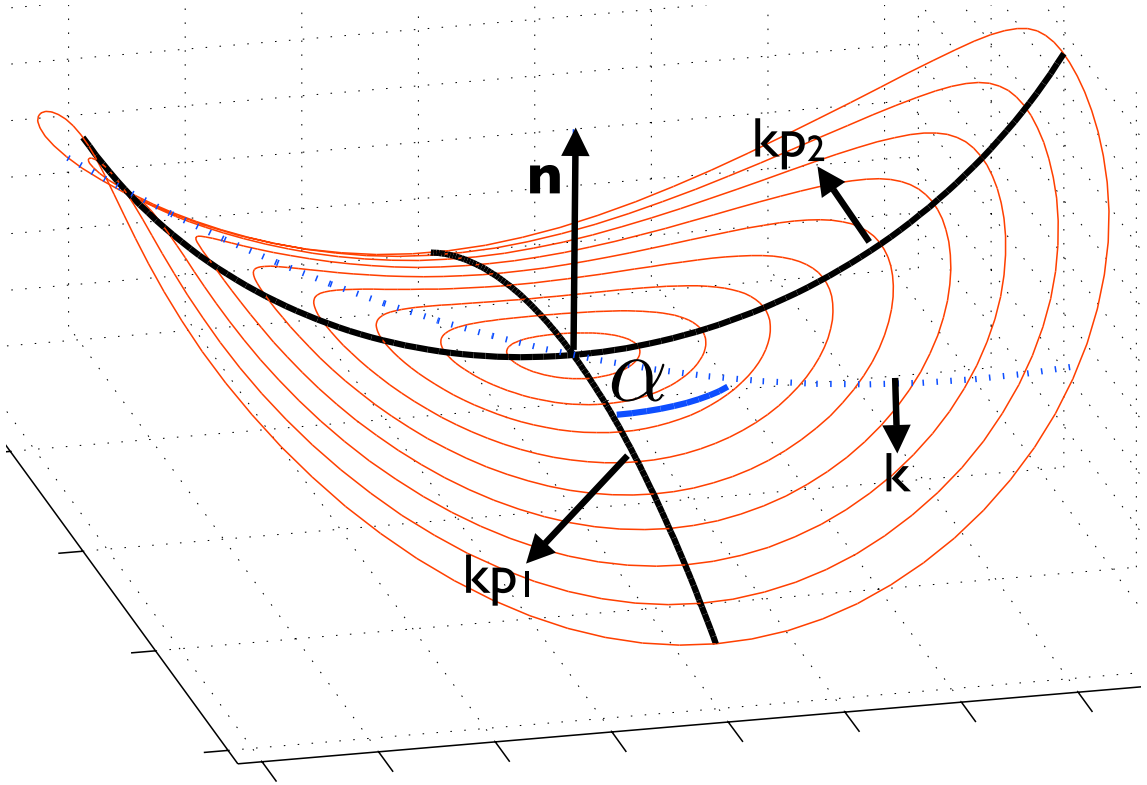


Fig. 6.2. A surface with the the two principal curvatures denoted by kp_1 and kp_2 . Also shown is another curvature k with an angle α with kp_1 .

end up with four points at the surface. The curvature between two crossing points is approximately given by

$$k = \frac{(\mathbf{n}_i - \mathbf{n}_j) \cdot (\mathbf{r}_i - \mathbf{r}_j)}{(\mathbf{r}_i - \mathbf{r}_j) \cdot (\mathbf{r}_i - \mathbf{r}_j)} \quad (6.7)$$

where \mathbf{n}_i is the boundary normal at \mathbf{r}_i . This relation should be reasonably correct when the curvature radius is larger than the distance between the two crossing points. By estimating the curvature for three or more pairs of spacecraft, kp_1 , kp_2 and α_0 can be found from Eq. 6.6.

Chapter 7

Summary of papers

7.1 Paper I: Cluster observations of a field aligned current at the dawn flank of a bursty bulk flow

This paper is an event study of a BBF which has the predicted properties of a depleted flux tube. The most characteristic feature of this event was a strong bipolar perturbation in the B_Z component together with enhancement in B_Y at the leading edge of the flow. Without more detailed examination, this could easily be identified as a flux rope according to the description in Sect. 4.1.3. However, more detailed examination revealed that the observations could be a result of the interaction of an earthward moving flux tube with the ambient plasma.

A comprehensive analysis of the BBF boundary was done. It was found that Cluster encountered the BBF from the dawn side in the outer CPS (see Fig. 5 in Paper I). It was a strong earthward FAC at the boundary. Thus, it was consistent with the BBF current wedge discussed in Sect. 3.1. The observations near the boundary generally agreed with those of *Sergeev et al.* (1996) (Sect. 4.1), but there were also some important differences. In Fig. 4.6 the plasma in front of the bubble is pushed sideways primarily in the Y direction. In our observations the plasma flow in front of the boundary was earthward, southward and dawnward. The flow was also strictly perpendicular to the magnetic field. The magnetic field was southward, dawnward and tailward. Careful considerations of the topology of the BBF boundary revealed that these observations were consistent with magnetic field lines which were draped around the flux tube as it moved earthward. It was also found that this draping, corresponded to the twisting of the magnetic field reported by *Birn et al.* (2004). (Sect. 3.1). It therefore supports their result, which showed that flow vortices are the main generation mechanism for field aligned currents during fast flows.

After the satellites had crossed the BBF boundary, the observations showed that the BBF had the predicted properties of a depleted flux tube. This included strong dipolarization, reduced density and increased temperature. The dipolarization was

strongest in the leading part of the flow and then gradually decreased.

These results are important because they support the model where bubbles can move earthward by displacing the flux tubes ahead rather than just compressing all the plasma in front of the bubble. It also demonstrates, as emphasised in Chapter 4, how important good selection criteria are for statistical studies in the magnetotail. Since the objects studied are inherently three dimensional structures which are evolving in time, it is essential to know exactly where the spacecraft are located when the observations are done. Finally, the results showed that BBFs can be important generators of FACs

This paper was written in close cooperation with a number of people. Of major importance was the contribution from H. Hasegawa. He did the Grad-Shafranov reconstruction and suggested text for the parts of the paper related to the reconstruction.

7.2 Paper II: The Hall current system revealed as a statistical significant pattern during fast flows

In this paper we wanted to examine whether the Hall current system in the reconnection region, couples to regions far away, or if it is closed in the immediate vicinity of the X-line. The Harris current sheet model (Sect. 6.1) was used to determine where the satellites were located in the current sheet. In that way, a coordinate Z relative to the current sheet center could be found for every magnetic field sample.

$$\frac{Z}{L} = \tanh^{-1} \left(\frac{B_X}{B_L} \right) \quad (7.1)$$

from Eq. 6.2. To identify the outflow region of an X-line, only events where $|V_X|$ exceeded 200 km/s for $|Z|/L < 0.2$ were selected. This criterion was based on the result from *Raj et al.* (2002) that all FABs were excluded for $B_X < 5$ nT (Sect. 4.1.1). This corresponds to $|Z|/L < 0.2$ for a lobe magnetic field of 25 nT. B_Y as a function of Z was estimated for each event. The derivative of B_Y with respect to Z was used to estimate the earthward and tailward currents. In the end, the average currents were calculated separately for earthward and tailward flows. A more detailed description of the method and the selection criteria is given in the paper.

The main result was that the earthward and tailward currents were in accordance with the Hall current system. There were currents towards the X-line in the center of the current sheet and currents away from the X-line closer to the lobes. The division between currents into and away from the X-line, was found at $B_X \approx 0.7B_L$, on average. This is slightly lower than *Asano et al.* (2004) who found the division at B_X/B_L between 0.8 and 0.85. A reason for this may be their criterion that the

ion density had to be lower than 0.1 cm^{-3} in the reconnection region. This may have biased their study to reconnection of open field lines, which would result in a separatrix close to the lobes. What is more interesting, is that we found the current towards the X-line to peak in the neutral sheet. This is in sharp contrast to the conclusions of *Nagai et al.* (2001, 2003) that the currents only existed near the separatrix. This indicate that the ions remain decoupled far away from the X-line in the outflow region. However, no attempt was done to estimate the distance from the X-line in our study. Thus, both currents close to the X-line and far away from it is mixed in the average pattern.

7.3 Paper III: Can magnetotail reconnection produce the observed ionospheric observations?

This is a statistical study based on 13 reconnection events. The reconnection events were identified by the quadrupolar pattern in B_Y produced by the Hall current system. The particle fluxes in the reconnection regions were measured by PEACE and RAPID on Cluster. Based on 1 min average spectra, the predicted UV and X-ray emissions in the ionosphere were estimated. It was found that the predicted auroral intensities were low. For 6 of the events global imaging data were available and predicted and observed emissions at Cluster footprint could be compared. The observed emissions were generally found to be more intense than predicted.

Since at least three of four Hall currents loops were observed in each event, it was very likely that Cluster passed through the reconnection regions. Given that the particle fluxes in the reconnection region only predicted low auroral intensities in the ionosphere, we concluded that there must be some other acceleration mechanism between the reconnection region and the conjugate ionosphere.

In Paper II it was shown statistically that the Hall current system can extend far away from the reconnection region. In Paper IV it was shown that this current system also can close in the ionosphere. It is therefore quite likely that the Hall current loops used to identify the reconnection regions, closed in the ionosphere. Also the fast flows from the reconnection region can generate field aligned currents as shown in Paper I. Field aligned currents can lead to potential drops near the Earth where the density is low and the mirror force is high (*Schriver et al.*, 2003, and references therein). If it is these potential drops that are the acceleration mechanism, it supports that the field aligned currents close in the ionosphere. In order to check this, the correlation coefficient between field aligned currents in and around the reconnection region and the AE index was estimated. This was also done for the magnitude of the fast flows and AE. There was no significant correlation between the field aligned currents in the reconnection region and AE. This may be because the effects of the Hall current system closing in the ionosphere is too weak or too localised to be measurable in a global index such as AE. However, there was weak correlation between AE and the magnitude of the fast flows.

This paper was written by N. Østgaard and my role in the paper has mainly been analysis and interpretation of the magnetospheric measurements.

7.4 Paper IV: Reconnection Hall current system observed in the magnetotail and in the ionosphere

This paper is an event study where Cluster observations in the magnetotail have been compared with measurements from the IMAGE magnetometer network near the ionospheric footprint of Cluster. The event was found by comparing a list of time intervals where Cluster and IMAGE were conjugate, with another list of events found by the same selection criteria as in Paper II.

In the magnetotail it was found a tailward current close to the neutral sheet and an earthward current closer to the lobes, in agreement with the result from Paper II. In the conjugate ionosphere, the magnetometer measurements were used to derive the equivalent currents. The equivalent current pattern was found to be consistent with that obtained if the currents observed in the magnetosphere closed in the ionosphere. These observations are the first direct measurements which show that the Hall current system can close in the ionosphere.

Interesting in this event is that the division between tailward and earthward currents is at B_X/B_L between 0.4 and 0.5, as seen from the peaks of B_Y in Fig. 2b-2e in Paper IV. According to the study by *Asano et al.* (2004), this indicates that Cluster is close to the reconnection region. Another result from their study was that the current sheet is bifurcated in the outflow region. Figure 7.1 shows a reconstruction of the cross tail current sheet by using the technique described in Sect. 6.3. This figure was not included in the paper. It can be seen that the current density peaks outside the neutral sheet ($Z = 0$), in accordance with a bifurcated current sheet. This supports the interpretation that Cluster are close to the reconnection region.

This paper would not have been possible without the contributions from L. Juusola and O. Amm who analysed the data from IMAGE and wrote the corresponding text.



Fig. 7.1. Reconstruction of the cross tail current sheet between 21:35 and 21:51 UT 07 Sep 2001

Bibliography

- Angelopoulos, V., W. Baumjohann, C. F. Kennel, F. V. Coroniti, M. G. Kivelson, R. Pellat, R. J. Walker, H. Lühr, and G. Paschmann (1992), Bursty bulk flows in the inner central plasma sheet, *J. Geophys. Res.*, *97*, 4027–4039.
- Angelopoulos, V., et al. (1994), Statistical characteristics of bursty bulk flow events, *J. Geophys. Res.*, *99*(A11), 21,257–21,280.
- Asano, Y., T. Mukai, M. Hoshino, Y. Saito, H. Hayakawa, and T. Nagai (2004), Current sheet structure around the near-Earth neutral line observed by Geotail, *J. Geophys. Res.*, *109*(A2), doi:10.1029/2003JA010114.
- Baker, D. N., T. I. Pulkkinen, V. Angelopoulos, W. Baumjohann, and R. L. McPherson (1996), Neutral line model of substorms: Past results and present view, *J. Geophys. Res.*, *101*(A6), 12,975–13,010.
- Balogh, A., et al. (2001), The Cluster Magnetic Field Investigation: Overview of in-flight performance and initial results, *Ann. Geophys.*, *19*, 1207–1217.
- Baumjohann, W., and R. A. Treumann (1997), *Basic Space Plasma Physics*, chap. 6, Imperial College Press, 57 Shelton Street, Covent Garden, London WC2H 9HE.
- Baumjohann, W., G. Paschmann, N. Sckopke, C. A. Cattell, and C. W. Carlson (1988), Average Ion Moments in the Plasma Sheet Boundary Layer, *J. Geophys. Res.*, *93*(A10), 11,507–11,520.
- Baumjohann, W., G. Paschmann, and C. A. Cattell (1989), Average Plasma Properties in the Central Plasma Sheet, *J. Geophys. Res.*, *94*(A6), 6597–6606.
- Baumjohann, W., G. Paschmann, and H. Lühr (1990), Characteristics of high speed ion flows in the plasma sheet, *J. Geophys. Res.*, *95*, 3801–3809.
- Birkeland, K. (1908), *The norwegian aurora polaris expedition, Volume I, First section*, H Aschehoug and Co, Christiania.
- Birkeland, K. (1913), *The norwegian aurora polaris expedition, Volume I, Second section*, H Aschehoug and Co, Christiania.

- Birn, J. (1987), Magnetotail equilibrium theory: The general three-dimensional solution, *J. Geophys. Res.*, *92*(A10), 11,101–11,108.
- Birn, J., and M. Hesse (2005), Energy release and conversion by reconnection in the magnetotail, *Ann. Geophys.*, *23*(10), 3365–3373.
- Birn, J., J. Raeder, Y. L. Wang, R. A. Wolf, and M. Hesse (2004), On the propagation of bubbles in the geomagnetic tail, *Ann. Geophys.*, *22*, 1773–1786.
- Brekke, A. (1997), *Physics of the upper polar atmosphere*, chap. 8, Wiley-Praxis series in atmospheric physics, John Wiley & Sons Ltd.
- Cao, J. B., et al. (2006), Joint observations by Cluster satellites of bursty bulk flows in the magnetotail, *J. Geophys. Res.*, *111*, A04,206, doi:10.1029/2005JA011322.
- Chen, C. X., and R. A. Wolf (1993), Interpretation of high-speed flows in the plasma sheet, *J. Geophys. Res.*, *98*(A12), 21,409–21,419.
- Chen, C. X., and R. A. Wolf (1999), Theory of thin-filament motion in the Earth’s magnetotail and its applications to bursty bulk flows, *J. Geophys. Res.*, *104*(A7), 14,613–14,626.
- Clemmow, P. C., and J. Dougherty (1969), *Electrodynamics of Particles and Plasmas*, Addison-Wesley series in advanced physics, Addison-Wesley Publishing Company.
- Cowley, S. W. H. (2000), Magnetosphere-ionosphere interactions: A tutorial review, in *Magnetospheric Current Systems*, *Geophys. Monogr. Ser.*, vol. 118, edited by S. Ohtani, R. Fujii, M. Hesse, and R. L. Lysak, pp. 91–106, AGU, 2000 Florida Avenue, N.W.; Washington, D.C. 20009.
- Cummings, W. D., and A. J. Dessler (1967), Field-aligned currents in the magnetosphere, *J. Geophys. Res.*, *72*(3), 1007–1013.
- Daly, P. W. (2002), *User’s Guide to the Cluster Science Data System*, European Space Agency, document Reference Number: DS-MPA-TN-0015.
- Dessler, A. J. (1984), The evolution of arguments regarding the existence of field-aligned currents, in *Magnetospheric Currents*, *Geophysical Monograph*, vol. 28, edited by T. A. Potemra, pp. 22–28, American Geophysical Union, 2000 Florida Avenue, N.W.; Washington, D.C. 20009.
- Dessler, A. J., and J. M. Wilcox (1970), Magnetic storms and the aurorae: A reprint of selected portions of a 1939 article by Hannes Alfvén, with marginal annotations., *Eos Trans. AGU*, *51*(3), 180–194.
- Dungey, J. W. (1961), Interplanetary magnetic field and the auroral zones, *Physical Review Letters*, *6*(2), 47–48.

- Egeland, A. (1984), Kristian Birkeland: The man and the scientist, in *Magnetospheric Currents, Geophysical Monograph*, vol. 28, edited by T. A. Potemra, pp. 1–16, American Geophysical Union, 2000 Florida Avenue, N.W.; Washington, D.C. 20009.
- Erickson, G. M., and R. A. Wolf (1980), Is steady convection possible in the earth’s magnetotail, *Geophys. Res. Lett.*, 7(11), 897–900.
- Escoubet, C. P., M. Fehringer, and M. Goldstein (2001), The Cluster mission, *Annales Geophysicae*, 19, 1197–1200.
- Fairfield, D. H. (1985), Solar wind control of magnetospheric pressure (cdaw 6), *J. Geophys. Res.*, 90(A2), 1201–1204.
- Haaland, S. E., G. Paschmann, M. Förster, J. M. Quinn, R. B. Torbert, C. E. McIlwain, H. Vaith, P. A. Puhl-Quinn, and C. A. Kletzing (2007), High-latitude plasma convection from Cluster EDI measurements: method and IMF-dependence, *Ann. Geophys.*, 25(1), 239–253.
- Harris, E. G. (1962), The equilibrium of oppositely directed magnetic fields, *Nuovo Cimento*, 23, 115–121.
- Harvey, C. C. (1998), Spatial gradients and the volumetric tensor, in *Analysis Methods for Multi-Spacecraft Data*, edited by G. Paschmann and P. W. Daly, ISSI Scientific Report, 1.1 ed., pp. 307–322, International Space Science Institute, Hallerstrasse 6, CH-3012 Bern, Switzerland.
- Hones Jr, E. W. (1984), Plasma sheet behavior during substorms, in *Magnetic Reconnection in Space and Laboratory Plasmas, Geophysical Monograph*, vol. 30, edited by E. W. Hones Jr, pp. 178–184, American Geophysical Union, 2000 Florida Avenue, N.W.; Washington, D.C. 20009.
- Hughes, W. J. (1995), The magnetopause, magnetotail, and magnetic reconnection, in *Introduction to Space Physics*, edited by M. G. Kivelson and C. T. Russell, chap. 9, pp. 227–287, Cambridge University Press.
- Hughes, W. J., and D. G. Sibeck (1987), On the 3-dimensional structure of plasmoids, *Geophys. Res. Lett.*, 14(6), 636–639.
- Iijima, T., and T. A. Potemra (1976), The Amplitude Distribution of Field-Aligned Currents at Northern High Latitudes Observed by Triad, *J. Geophys. Res.*, 81(13), 2165–2174.
- Khrabrov, A. V., and B. U. Ö. Sonnerup (1998a), dehoffmann-teller analysis, in *Analysis Methods for Multi-Spacecraft Data*, edited by G. Paschmann and P. W. Daly, pp. 221–248, International Space Science Institute, Hallerstrasse 6, CH-3012 Bern, Switzerland.

- Khrabrov, A. V., and B. U. Ö. Sonnerup (1998b), Error estimates for minimum variance analysis, *J. Geophys. Res.*, *103*(A4), 6641–6651.
- Lui, A. T. Y., and Y. Kamide (2003), A fresh perspective of the substorm current system and its dynamo, *Geophys. Res. Lett.*, *30*(18), doi:10.1029/2003GL017835.
- McPherron, R. L., C. T. Russel, and M. P. Aubry (1973), Satellite Studies of Magnetospheric Substorms on August 15, 1968 9. Phenomenological Model for Substorms, *J. Geophys. Res.*, *78*(16), 3131–3149.
- Mottez, F., and G. Chanteur (1994), Surface crossing by a group of satellites: A theoretical study, *J. Geophys. Res.*, *99*(A7), 13,499–13,507.
- Nagai, T., and S. Machida (1998), Magnetic Reconnection in the Near-Earth Magnetotail, in *New Perspectives on the Earth's Magnetotail, Geophysical Monograph*, vol. 105, pp. 211–224, American Geophysical Union.
- Nagai, T., I. Shinohara, M. Fujimoto, M. Hoshino, Y. Saito, S. Machida, and T. Mukai (2001), Geotail observations of the Hall current system: Evidence of magnetic reconnection in the magnetotail, *J. Geophys. Res.*, *106*(A11), 25,929–25,949.
- Nagai, T., I. Shinohara, M. Fujimoto, S. Machida, R. Nakamura, Y. Saito, and T. Mukai (2003), Structure of the Hall current system in the vicinity of the magnetic reconnection site, *J. Geophys. Res.*, *108*(A10), doi:10.1029/2003JA009900.
- Nagai, T., et al. (1998), Structure and dynamics of magnetic reconnection for substorm onsets with Geotail observations, *J. Geophys. Res.*, *103*(A3), 4419–4440.
- Nakamura, M., G. Paschmann, W. Baumjohann, and N. Sckopke (1992), Ion Distributions and Flows in and Near the Plasma Sheet Boundary Layer, *J. Geophys. Res.*, *97*(A2), 1449–1460.
- Nakamura, M. S., M. Fujimoto, and K. Maezawa (1998), Ion dynamics and resultant velocity space distributions in the course of magnetotail reconnection, *J. Geophys. Res.*, *103*(A3), 4531–4546.
- Nakamura, R., et al. (2002), Fast flow during current sheet thinning, *Geophys. Res. Lett.*, *29*(23), 2140, doi:10.1029/2002GL016200.
- Nakamura, R., et al. (2004a), Flow shear near the boundary of the plasma sheet observed by cluster and geotail, *J. Geophys. Res.*, *109*, A05,204, doi:10.1029/2003JA010174.
- Nakamura, R., et al. (2004b), Spatial scale of high-speed flows in the plasma sheet observed by Cluster, *Geophys. Res. Lett.*, *31*, L09,804, doi:10.1029/2004GL019558.

- Nakamura, R., et al. (2005), Localized fast flow disturbance observed in the plasma sheet and in the ionosphere, *Ann. Geophys.*, *23*, 553–566.
- Ohtani, S., S. Kokubun, R. C. Elphic, and C. T. Russel (1988), Field-aligned current signatures in the near-tail region 1. ISEE observations in the plasma sheet boundary layer, *J. Geophys. Res.*, *93*(A9), 9709–9720.
- Ohtani, S., M. A. Shay, and T. Mukai (2004), Temporal structure of the fast convective flow in the plasma sheet: Comparison between observations and two-fluid simulations, *J. Geophys. Res.*, *109*, A03,210, doi:10.1029/2003JA010002.
- Parks, G. K. (2004), *Physics of Space Plasmas, An Introduction*, chap. 7, Advanced Book Program, second ed., Westview Press.
- Paterson, W. R., L. A. Frank, S. Kokubun, and T. Yamamoto (1998), Geotail survey of ion flow in the plasma sheet: Observations between 10 and 50 R_E , *J. Geophys. Res.*, *103*(A6), 11,811–11,825.
- Pontius, D. H., and R. A. Wolf (1990), Transient flux tubes in the terrestrial magnetosphere, *Geophys. Res. Lett.*, *17*(1), 49–51.
- Raj, A., T. Phan, R. P. Lin, and V. Angelopoulos (2002), Wind survey of high-speed bulk flows and field-aligned beams in the near-earth plasma sheet, *J. Geophys. Res.*, *107*(A12), 1419, doi:10.1029/2001JA007547.
- Rème, H., et al. (2001), First multispacecraft ion measurements in and near the earth’s magnetosphere with the identical cluster ion spectrometry (cis) experiment, *Ann. Geophys.*, *19*, 1303–1354.
- Runov, A., et al. (2005), Reconstruction of the magnetotail current sheet structure using multi-point cluster measurements, *Planet. Space Sci.*, *53*, 237–243, doi:10.1016/j.pss.2004.09.049.
- Schödel, R., W. Baumjohann, R. Nakamura, and V. A. S. T. Mukai (2001), Rapid flux transport in the magnetotail, *J. Geophys. Res.*, *106*(A1), 301–313.
- Schrifer, D., M. Ashour-Abdalla, R. J. Strangeway, R. L. Richard, C. Klezting, Y. Dotan, and J. Wygant (2003), FAST/Polar conjunction study of field-aligned auroral acceleration and corresponding magnetotail drivers, *J. Geophys. Res.*, *108*(A9), 8020, doi:10.1029/2002JA009426.
- Sergeev, V. A., R. C. Elphic, F. S. Mozer, A. Saint-Marc, and J. A. Sauvaud (1992), A two-satellite study of nightside flux transfer events in the plasma sheet, *Planet. Space Sci.*, *40*, 1551–1672.
- Sergeev, V. A., V. Angelopoulos, J. T. Gosling, C. A. Cattell, and C. T. Russel (1996), Detection of localized, plasma-depleted flux tubes or bubbles in the midtail plasma sheet, *J. Geophys. Res.*, *101*(A5), 10,817–10,826.

- Sergeev, V. A., M. V. Kubyshkina, K. Liou, P. T. Newell, G. Parks, R. Nakamura, and T. Mukai (2001), Substorm and convection bay compared: Auroral and magnetotail dynamics during convection bay, *J. Geophys. Res.*, *106*(A9), 18,843–18,855.
- Sergeev, V. A., D. A. Sormakov, W. Baumjohann, R. Nakamura, A. V. Runov, T. Mukai, and T. Nagai (2006), Survey of large-amplitude flapping motions in the midtail current sheet, *J. Geophys. Res.*, *24*(7), 2015–2024.
- Sharma, A. S., et al. (2008), Transient and localized processes in the magnetotail: a review, *Ann. Geophys.*, *26*, 955–1006.
- Shay, M. A., J. F. Drake, and M. Swisdak (2007), Two-scale structure of the electron dissipation region during collisionless magnetic reconnection, *Phys Rev Lett*, *99*(15), doi:10.1103/PhysRevLett.99.155002.
- Shiokawa, K., W. Baumjohann, and G. Haerendel (1997), Braking of high-speed flows in the near-Earth tail, *Geophys. Res. Lett.*, *24*(10), 1179–1182.
- Siscoe, G. L., L. Davis Jr, P. J. Coleman Jr, E. J. Smith, and D. E. Jones (1968), Power spectra and discontinuities of the interplanetary magnetic field: Mariner 4, *J. Geophys. Res.*, *73*(1), 61–82.
- Slavin, J. A., E. J. Smith, D. G. Sibeck, D. N. Baker, and S.-I. Akasofu (1985), An ISEE 3 study of average and substorm conditions in the distant magnetotail, *J. Geophys. Res.*, *90*(A11), 10,875–10,895.
- Slavin, J. A., et al. (2003), Geotail observations of magnetic flux ropes in the plasma sheet, *J. Geophys. Res.*, *108*(A1), 1015, doi:10.1029/2002JA009557.
- Snekvik, K. (2005), Plasma Sheet Dynamics in the Mid Magnetotail, Cand. scient. thesis, University of Bergen.
- Sonnerup, B. U. Ö. (1979), Magnetic field reconnection, *Solar System Plasma Physics, III*, 45–108.
- Treumann, R. A., C. H. Jaroschek, R. Nakamura, A. Runov, and M. Scholera (2006), The role of the hall effect in collisionless magnetic reconnection, *Adv. Space Res.*, *38*, 101–111, doi:10.1016/j.asr.2004.11.045.
- Ueno, G., S. Ohtani, T. Mukai, Y. Saito, and H. Hayakawa (2003), Hall current system around the magnetic neutral line in the magnetotail: Statistical study, *J. Geophys. Res.*, *108*(A9), 1347, doi:10.1029/2002JA009733.
- Yamade, Y., M. Fujimoto, N. Yokokawa, and M. S. Nakamura (2000), Field-aligned currents generated in magnetotail reconnection: 3D Hall-MHD simulations, *Geophys. Res. Lett.*, *27*(8), 1091–1094.

Appendix A

Abbreviations and Acronyms

AGSM	Aberrated GSM
BBF	Bursty Bulk Flow
CIS	Cluster Ion Spectrometry
CODIF	COmposition and DIstribution Function analyser
CPS	Central Plasma Sheet
CTC	Cross Tail Current
DNL	Distant Neutral Line
DMSP	Defense Meterological Satellite Program
FAB	Field Aligned Beam
FAC	Field Aligned Current
FGM	Fluxgate Magnetometer
GSE	Geocentric Solar Ecliptic coordinate system
GSM	Geocentric Solar Magnetospheric coordinate system
HIA	Hot Ion Analyser
IMAGE	Imager for Magnetopause- to-Auroral Global Exploration
IMAGE	International Monitor for Geomagnetic Effects
IMF	Interplanetary Magnetic Field
MHD	Magneto Hydro Dynamics
NENL	Near-Earth Neutral Line
NFTE	Night-side Flux Transfer Event
NS	Neutral Sheet
PSBL	Plasma Sheet Boundary Layer
RFT	Rapid Flux Transport
R_E	Radius of the Earth
SEA	Superposed Epoch Analysis
SMC	Steady Magnetospheric Convection

Index

- Kp* index, 36
- acceleration region, 11, 25
- adiabatic relation, 12
- AGSM, 10
- aurora, 2, 36
- Birkeland, Kristian, 2
- boundary layer model, 24
- braking of flow, 18, 26
- bubble, *see* depleted flux tube
- bulk flows, 25
- bursty bulk flow, 13, 24, 35
- closed field line, 9
- Cluster, 1, 39
- Cluster Ion Spectrometry, 41
- CODIF, 41
- convection, 8, 9, 26
- current sheet, 19, 43
 - bifurcated, 30, 33
 - Harris, 45
 - orientation, 46
 - reconstruction, 45
- current wedge, 17
- curvature force, 8, 13
- deHoffmann-Teller analysis, 47
- depleted flux tube, 13, 18, 30
- diamagnetic current, 17
- diffusion region
 - electron, 19
 - ion, 19, 31
- dipolarization, 14
- elevation angle, 26
- field aligned beam, 12, 24
- field aligned current, 4, 17, 20, 30, 35
- flux pile-up, 18
- flux rope, 14, 29
- flux transport, *see* convection
- flux tube, 12
- fluxgate magnetotometer, 41
- frozen-in approximation, 8, 19
- generator, 17, 19
- GSE, 10
- GSM, 10
- gyro period, 8
- gyro radius, 8, 19
- gyrotropic distribution, 8
- Hall current, 19, 31, 35
- HIA, 41
- inertial current, 17
- inertial length, 19
- inflow region, 8
- load, 17
- lobe, 9, 11, 14
- magnetotail, 11
- meridional current system, 21
- momentum equation, 8
- neutral line, 9
 - distant, 14
 - near-Earth, 14
- neutral sheet, 11, 44
- night side flux transfer event, 29

open field line, 9
outflow region, 8

particle flux, 41
phase space density, 7, 41
plasma β , 44
plasma sheet, 11
 boundary layer, 11, 25, 44
 central, 11, 25
 inner, 24
 inner central, 24, 44
 outer, 24
 outer central, 24, 44
plasmoid, 14
polar cap, 9
pressure balance, 44
pressure crisis, 12
principal curvature, 47

quadrupolar pattern, 19, 33

rapid convection event, 26
reconnection, 8, 14, 19, 29, 43
 near-Earth, 14, 30
region 1 and 2, 36

separatrix, 9, 33
space charge, 18
substorm, 2
superposed epoch analysis, 27

terrella experiment, 4

variance analysis, 46
Vlasov equation, 7
vortex, 18

X-line, 9, *see* reconnection
 distant, 11

